UCLouvain

FACULTE DES SCIENCES

Faculté des sciences

Analysis of the W-Boson Mass anomaly with a 4-fermion operator

Mémoire présenté en vue de l'obtention du grade académique de
Master [120] en sciences physiques

Auteur : Thomas Cousin
Promoteur : Prof. Céline Degrande
Lecteurs : Prof. Christophe Delaere, Prof. Fabio Maltoni
École de Physique
Année académique 2022-2023

Acknowledgement

First of all, I would like to thank Prof. Céline Degrande for accepting to be my supervisor. Her guidance, patience and availability were always a great help. In addition her advises have been also a source of inspiration and progression.

I would also like to thank Prof. Christophe Delaere and Prof. Fabio Maltoni for accepting to be my readers and the time they have accorded to me. There commentaries and advises pushed me forward.

Thanks as well to the CP3 and EFT teams for the discussions and the help offered. Meetings shared with them have always been a source of inspiration and a moment to ask freely for help.

I also address a warm thank you to Alisée B., Romain G., Quentin H. and Alice L. for the moments of sharing and discussion.

Finally, I would like to thank my family and friends for supporting and encouraging me during these past months.

Contents

List of Figures

List of Tables

Acronyms

BEH Brout Englert Higgs.

BSM Beyond Standard Model.

CDF Collider Detector at Fermilab.

EFT Effective Field Theory.

EW Electroweak.

LHC Large Hadron Collider.

MC Monte Carlos.

NP New Physics.

pdf Parton distribution function.

QCD Quantum chromodynamics.

QFT Quantum Field Theory.

SM Standard Model.

SMEFT Standard Model Effective Field Theory.

SSB Spontaneous symmetry breaking.

UFO Universal FeynRules Output.

UV Ultraviolet.

vev Vaccuum expectation value.

1 Introduction

The standard model of particle physics is the model used by physicists to describe three of the four fundamental forces at the microscopic level. These interactions are the electromagnetism, the weak and the strong interactions. It predicts also the existence of elementary particles, the most fundamental pieces of nature. Initially postulated by the Nobel Prize laureates Sheldon Lee Glashow, Abdus Salam and Steven Weinberg, the W boson is one of them. Responsible for the radioactive decay, it has been observed for the first time at CERN by Carlo Rubbia and Simon van der Meer also awarded by the Nobel Prize. Since, its discovery, physicists continued to measure with precision its mass. Until recently, every measurement was in accord with the standard model prediction. But in April 2022, an experimental collaboration (CDF II) published in Science Magazine a high precision measurement that appeared to be in tension with the standard model.

It is well known by the scientific community that the standard model is not complete. Besides the gravitational force, one can quote the dark matter, dark energy, neutrino masses that are not explained by the standard model. This has led physicists to investigate extensions of the latter. In collider physics, it is commonly assumed that new physics takes place at higher energy. In this case, one uses effective field theories to model the effect of high energy physics at smallest scales. The first possibility is to assume that the predicted mass of the W-boson is modified by new physics contribution. This approach has been investigated in the literature, for example in Ref.[21]. The second possibility is to assume that the mass is not changed. The main idea of the collaboration is to use distributions to fit the mass. One may assume that new physics, one way or another, changes the distributions used to determine the W-mass. Therefore, in this master thesis, we numerically investigate the effect of a effective field theory approach related to the new mass measurement of the W boson. We also investigate the possibility to deceive a mass fit.

The first section focuses on the theoretical aspects. We present the Standard model of particle physics. Then we talk about the effective field theories and the standard model effective field theory. We also give an historical example, the Fermi's theory. We continue with a presentation of the Tevatron and the CDF II collaboration. We also give an historical overview of the W boson, its measurement and its keystone position in the standard model and possible new physics extensions. We conclude with the presentation of the model used in this master thesis and the motivations to perform this analysis.

The second section describes the methodology followed in this work. We begin with the construction of the model. Then we generate the standard model distributions and the new physics distributions. We verify whether or not distributions are modified when new physics is turned on. We continue with the fitting strategy used to fit the mass. This fit allows us to find the best fitted mass of the distribution and its corresponding confidence interval.

The last section is devoted to the presentation and the discussion of the results. We generate different distributions for increasing contribution of new physics and for each of them we perform a fit. We then try to use the linearity of the new physics contribution. This allows to quantify the value of this contribution needed to give the shift observed by the CDF II collaboration. We check if this value is in agreement with some analysis performed in the literature. We finally discuss the effect of this new physics contribution on other parameters of the standard model related to the W-mass prediction.

2 Theory

2.1 Standard Model

At the beginning of the 20th century, mechanics and gravity were described by Newton's and Galileo's laws, electromagnetism by Maxwell, statistical theories by Boltzmann and Van der Waals and thermodynamics by Carnot and Clausius. Legend tells that Lord Kelvin would have said, "In the clear blue sky of physics there remained on the horizon just two small clouds of incomprehension that obscured the beauty and clearness". It seemed that studying physics became useless, since the resolution of those two problems was supposed to be a matter of time. Fortunately, these two small clouds led to two revolutions: quantum mechanics and relativity (special and general).

These revolutions built the theoretical pillars of the modern physics. In parallel to theoretical discoveries, experiments where conducted to probe the atom, seeking the elementary pieces of nature. In addition to the already known interactions, electromagnetism and gravitation, these experiments showed the existence of two new interactions. The first one, the weak interaction, responsible of radioactive decays, was discovered by Pauli. The second, the strong interaction, responsible of nucleous cohesion, was postulated by Hideki Yukawa, a Japanese physicist. He introduced a new massive particle as the messenger of the strong interaction: the meson. This idea of a massive particle mediating the strong interaction to explain its short-ranged property is a key idea of the so-called Standard Model (SM). The latter is the results of decades and thousands of scientists working to build a model which explains three fundamental interactions, strong, weak and electromagnetism. Only the gravitational interaction escapes this model.

The standard model is built on Quantum Field Theories (QFT's), that are the quantum mechanics of infinitely many degrees of freedom objects. They are characterized by three pillars, quantum mechanics, Poincaré group and gauge symmetries. From Poincaré group we know that nature is composed of two types of particles, fermions and bosons (see Fig. 1). Fermions are the particles of matter and are subdivided into two classes, quarks and leptons. Quarks are coloured particles, since we don't observe any large coloured object, they have to be confined. There are six quarks' flavours (up, down, charm, strange, top and bottom) and three colours (blue, red, green). In addition, they have non integer electric charges, meaning that they form either mesons or hadrons with respectively two and three quarks . In opposition, leptons are not coloured, so they can be observed alone. Like quarks, there are six flavours of fermions, three charged (electron, muon, tau) and three neutral (electronic neutrino, muonic neutrino, tauic neutrino). Fermions are separated into three generations, the first one is the generation of the ordinary matter, proton and neutron being composed of up and down quarks. Note that the hierarchy of these generations is still a mystery. Finally, every particle comes in two different chirality, left-handed and right-handed, except neutrinos because they are massless in the standard model. Each particle has also an antimatter correspondent [36] [32].

From the third pillar of QFT's, in particle physics we implement interactions by imposing gauge symmetries. Therefore, forces are no longer mediated by something immaterial but by gauge bosons, in other words by the exchange of virtual particles. These particles interact with fermions via their charges. The mediator of the electromagnetic interaction, the photon (γ), interacts with all electrically charged particles. The mediators of strong interaction are the gluons (g). They are coloured charged and interact with coloured particles. The last 3 gauge bosons ($W^{\pm}$ and Z^0) are responsible for the

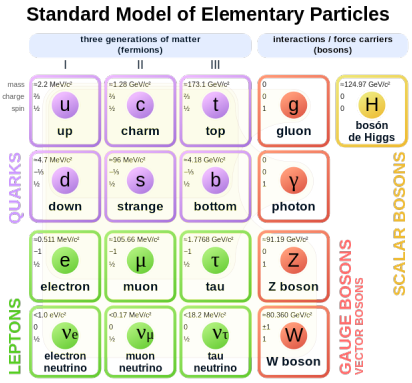

Figure 1: Standard Model [35]

weak interaction and interact with flavoured particles because of their weak charge. For example, as shown in Fig.2a, when a neutron decays, an up quark turns into a down by the producing a W boson which decays into an electron and its corresponding neutrino. Another example, the muon decay is also shown in Fig.2b [36] [32].

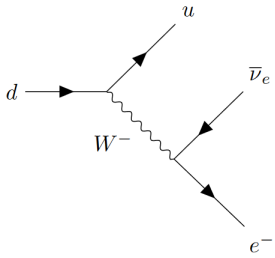

(a) Neutron decay

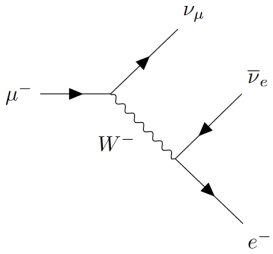

(b) Muon decay

Figure 2: Examples of processes in the standard model involving the W boson

From a group theory point of view, one can associate to each interaction a gauge group, U(1) for electromagnetism, SU(2) and SU(3) for the weak and strong interaction respectively. By identifying this group, one can find every of their properties. Nevertheless, one problem arises from these gauge symmetries. It prevents the existence of explicit masses in the Lagrangian, the mathematical expression that describes the model. However, we observe masses for almost all fermions. In addition, since weak and strong forces are short-ranged, in the Yukawa picture, one can assume that their gauge bosons are massive. Hence, physicists have developed two mechanisms that solved this problem. First, for the strong interaction by postulating the confinement of colours. The second is the Brout-Englert-Higgs (BEH) mechanism, which uses spontaneous symmetry breaking (SSB) to give masses to fermions as well as weak bosons. Wu's experiment shows that the weak interaction do not talk to right-handed particles and left-handed antiparticles. Chien-Shiung Wu studied the beta decay of the nickel, ${}^{60}_{27}Co \rightarrow {}^{60}_{28}Ni + e^- + \bar{\nu}_e + 2\gamma$ and in particular the emission of the electron in a magnetic field. Changing

the field direction changes the parity, she observed an asymmetry in the electron's production when changing the magnetic field direction. This means that the emission of left-handed particle is preferred by the weak interaction [36] [32].

We can now describe the standard model by paying attention to all the problems listed above. We begin with its gauge group,

$$SU(3)_c \otimes SU(2)_L \otimes U(1)_Y.$$

SU(3) is for the QCD part and it has height generators (g^a_μ, a =1,..., 8). The two others are for the electroweak (EW) part. The QED-like group, $U(1)_Y$, with the hypercharge (Y), has one generator (a_μ). SU(2) has three generators (b^i_μ, $i = 1, 2, 3$) . Following the Wu's experiment results, we can now write left-handed particles as doublet and right-handed particles as singlet, so they cannot interact weakly,

$$\begin{pmatrix} u \\ d \end{pmatrix}_L, \begin{pmatrix} c \\ s \end{pmatrix}_L, \begin{pmatrix} t \\ b \end{pmatrix}_L, \begin{pmatrix} \nu_e \\ e^- \end{pmatrix}_L, \begin{pmatrix} \nu_\mu \\ \mu^- \end{pmatrix}_L, \begin{pmatrix} \nu_\tau \\ \tau^- \end{pmatrix}_L,$$

$$u_R,\ d_R,\ c_R,\ s_R,\ t_R,\ b_R,\ e^-_R,\ \mu^-_R,\ \tau^-_R.$$

The first row has a weak charge because these particles are interacting with weak bosons, $I_0^{(3)} = +(-)1/2$ for the top (bottom) position. The second row has a weak null charge, $I_0^{(3)} = 0$. The hypercharge assignment is $Y_L = -1$, $Y_{\nu_R} = 0$ and $Y_{e_R} = -2$. The Table 1 gives the content of the standard model and their charges under different gauge groups. The electric charge is determined by the Gell-Mann–Nishijima formula,

$$Q = I_0^{(3)} + \frac{Y}{2}. \tag{1}$$

In order to generate masses, we need to implement BEH mechanism which leaves the gluons and the photon massless,

$$SU(3)_c \otimes SU(2)_L \otimes U(1)_Y \to SU(3)_c \otimes U(1)_{EM}.$$

The Higgs mechanism is characterized by two complex scalar fields,

$$\Phi = \frac{1}{\sqrt{2}} \begin{pmatrix} \phi^+ \\ \phi^0 \end{pmatrix} = \frac{1}{\sqrt{2}} \begin{pmatrix} \phi_1 + i\phi_2 \\ \phi_3 + i\phi_4 \end{pmatrix}, \tag{2}$$

In the broken phase, the doublet becomes,

$$\Phi = \frac{1}{\sqrt{2}} \begin{pmatrix} 0 \\ v \end{pmatrix}, \tag{3}$$

where $v = \sqrt{\frac{-\mu^2}{\lambda}}$. We can rewrite the real part of the neutral component of the Higgs doublet in terms of v and a field without expectation value,

$$\Phi = \frac{1}{\sqrt{2}} \begin{pmatrix} \phi_1 + i\phi_2 \\ v + H + i\phi_4 \end{pmatrix}, \tag{4}$$

where ϕ_1, ϕ_2 and ϕ_4 are the Goldstone bosons related to each symmetry broken in the broken phase. In the unitary gauge, Goldstones are not explicit but hidden in the longitudinal polarization of massive gauge bosons, we say that they have been "eaten" by gauge fields. In this gauge, the Higgs doublet is

$$\Phi' = \frac{1}{\sqrt{2}} \begin{pmatrix} 0 \\ v + H \end{pmatrix}, \tag{5}$$

at the end we are left with a degree of freedom that hasn't been absorbed by gauge bosons, this is a physical particle, known as the Higgs boson [36] [32].

We write now the Lagrangian of the standard model, that can be subdivided in sectors, QCD, EW, Higgs and Yukawa,

$$\mathcal{L}_{SM} = \mathcal{L}_{QCD} + \mathcal{L}_{EW} + \mathcal{L}_H + \mathcal{L}_y. \tag{6}$$

Note that we are using natural units where $\hbar = c = 1$ and every units are expressed in term of energy. The fist term of Eq.6, Quantum Chromodynamics, describes the strong interaction,

$$\mathcal{L}_{QCD} = -\frac{1}{4} G^a_{\mu\nu} G^{\mu\nu}_a + \bar{Q}_l (i \not{D}) Q^l + \bar{u}_{R,l} (i \not{D}) u^l_R + \bar{d}_{R,l} (i \not{D}) d^l_R, \tag{7}$$

where l is for fermions' generations. We can find the dynamics of the gauge fields, the kinetics of the quarks, the interaction of the gauge fields with themselves. To implement interactions between quarks and gauge fields we choose the form of D, the covariant derivative for the QCD part, as $D_\mu = \partial_\mu + g_3 \overrightarrow{\lambda} \cdot \overrightarrow{g}_\mu$, where λ are the Gell-Mann matrices and $Tr(\lambda_a \lambda_b) = 2\delta_{ab}$. The second term of Eq.6, the electroweak sector, unifies the electromagnetic and weak interaction,

$$\begin{aligned} \mathcal{L}_{EW} = -\frac{1}{4} W^i_{\mu\nu} F^{\mu\nu}_i - \frac{1}{4} B_{\mu\nu} B^{\mu\nu} + \bar{L}_l (i \not{D}) L^l + \bar{e}_{R,l} (i \not{D}) e^l_R + \bar{\nu}_{R,l} (i \not{D}) \nu^l_R \\ + \bar{Q}_l (i \not{D}) Q^l + \bar{u}_{R,l} (i \not{D}) u^l_R + \bar{d}_{R,l} (i \not{D}) d^l_R, \end{aligned} \tag{8}$$

where l is for the fermions' generation and $D_\mu = \partial_\mu + i \frac{g_2}{2} \overrightarrow{\tau} \cdot \overrightarrow{b}_\mu + i \frac{g_1}{2} Y_\phi a_\mu$ with g_1 and g_2 coupling constants of $U(1)_Y$ and $SU(2)_L$ respectively and $Tr(\tau_a \tau_b) = 2\delta_{ab}$. The two first term are kinetics terms for gauge fields and the three last terms are for the kinetics of fermions and their interaction with gauge fields. The third term of Eq.6 is the Lagrangian of the higgs doublet,

$$\mathcal{L} = (\mathrm{D}_\mu \phi)^\dagger (\mathrm{D}^\mu \phi) - V(\phi)^2 \tag{9}$$

where $V(\phi) = \mu^2 \phi^\dagger \phi + \lambda (\phi^\dagger \phi)^2$ the Higgs potential. If we develop the Higgs Lagrangian with the expression of Φ' in (5) we find that,

$$\begin{cases} W^\pm_\mu = \frac{b^1_\mu \mp i b^2_\mu}{\sqrt{2}} & \text{and} \quad m_W = \frac{g_2 v}{2} \\ Z^0_\mu = \frac{-g_1 a_\mu + g_2 b^3_\mu}{\sqrt{g_1^2 + g_2^2}} & \text{and} \quad m_Z = \sqrt{g_1^2 + g_2^2} \frac{v}{2} \\ A^0_\mu = \frac{g_2 a_\mu + g_1 b^3_\mu}{\sqrt{g_1^2 + g_2^2}} & \text{and} \quad m_A = 0 \end{cases} .$$

The model predicts the existence of three massive gauge vectors, two charged and one neutral, and one massless, the photon. Since no mechanism fixes the value of the coupling constant, the standard model do not predict the value of masses. Note that $m_Z > m_W$ and Z and A are mixing of b^3 and a. The mixing angle is given by $\frac{m_W}{m_Z} = cos(\theta_W)$, where θ_W is called the Weinberg angle. The electric charge is now determined by θ_W, $g_1 cos(\theta_W) = g_2 sin(\theta_W) = e$. The existence of a massive scalar boson is also predicted with the free mass m_H, and the muon decay fixes the vacuum expectation value (vev),

$$m_H = 2\lambda v^2 \qquad \text{and} \qquad v = \frac{1}{\sqrt{\sqrt{2}G_F}} = 246\ GeV$$

where $G_F = 1.16638 \times 10^{-5} GeV^{-2}$ is the Fermi constant. The last sector, the Yukawa sector gives mass to fermions,

$$\mathcal{L}_y = -y_l \bar{L}^l \phi e_R^l - Y_{lm}^d \bar{Q}^l \phi d_R^m - Y_{lm}^u \bar{Q}^l \tilde{\phi} u_R^m + h.c., \tag{10}$$

where l, m are generation indices, Y_{lm}^u and Y_{lm}^d are Yukawa couplings for up and down component respectively, y_l are Yukawa couplings for charged leptons and $\tilde{\phi} = i\sigma_2 \phi^*$. In the broken phase, this Lagrangian generates mass for fermions. In order to get physical state for quarks, we need to diagonalize Yukawa couplings matrices Y^u and Y^d,

$$M_u = V_L^u Y^u V_R^{u\dagger} \quad \text{and} \quad M_d = V_L^d Y^d V_R^{d\dagger}$$

This unitary transformation defines the quark mixing matrix, the CKM matrix, which gives the coupling constants of mass eigenstate with charged-current,

$$V_{CKM} = V_L^{u\dagger} V_L^d \qquad \Rightarrow \qquad \begin{pmatrix} d' \\ s' \\ b' \end{pmatrix} = \begin{pmatrix} V_{ud} & V_{us} & V_{ub} \\ V_{cd} & V_{cs} & V_{cb} \\ V_{td} & V_{ts} & V_{tb} \end{pmatrix} \begin{pmatrix} d \\ s \\ b \end{pmatrix}$$

where d, s, b are the mass eigenstates and d', s', b' are the flavour eingenstates. We should also note that every coupling constant with the Higgs is, in fact, proportional to the mass of the particle interacting for fermions and proportional to the square of the mass for gauge bosons,

$$g_{eH} = \frac{m_e}{v}, \qquad g_{WWH} = \frac{m_W^2}{v} \qquad \text{and} \qquad g_{ZZH} = \frac{m_Z^2}{v}.$$

We focus now on the 19 parameters of the standard model. First, we have the 9 coupling constants of fermions' masses. Then we have the gauge couplings g_1, g_2 determined by m_W, m_Z. The parameters of higgs potential (λ, μ) are given by m_h and v (vev). The CKM matrix has 4 parameters, 3 angles and one phase. Finally, the last two parameters are given by the strong sector, g_3 the coupling of the gauge field and θ_{QCD} that control the CP violation [36] [32].

$Fields$	$SU(3)_c$	$SU(2)_L$	$U(1)_Y$	$SO^+(3,1)$
$Q_i = (u_L^i, d_L^i)^T$	3	2	1/6	$(1/2, 0)$
$u_i = u_R, c_R, t_R$	3	1	2/3	$(0, 1/2)$
$d_i = d_R, s_R, b_R$	3	1	$-1/3$	$(0, 1/2)$
$L_i = (\nu_L^i, l_L^i)^T$	1	2	$-1/2$	$(1/2, 0)$
$l_i = e_R, \mu_R, \tau_R$	1	2	-1	$(0, 1/2)$
H	1	2	1/2	$(0, 0)$
$G_{\mu\nu}$	8	1	0	$(1, 0) \oplus (0, 1)$
$W_{\mu\nu}$	1	3	0	$(1, 0) \oplus (0, 1)$
$B_{\mu\nu}$	1	1	0	$(1, 0) \oplus (0, 1)$

Table 1: Group representation of the SM content

In this section, we have developed the standard model and showed its success. Despite the tremendous number of discoveries and the strongness of this model, scientific community is far from having eluded all mysteries of the nature. For example, dark matter and dark energy escape our understanding. Some attempts to explain dark matter use particle physics like WIMP's (Weakly Interactive Massive Particles) or axions. One can quote the neutrino mass that is zero in the SM but nonzero from experiment, since they oscillate. However the most compelling argument is the gravity at the quantum level. In the quest of explanation, one can consider some specific models to solve this problem. One can also consider a more humble approach: Effective Fields Theories.

2.2 Effective Field Theory

Effective Theories are used to capture the relevant information to describe a problem instead of using the full/exact theory (UV theory). For example, we don't need to describe precisely the motion of quarks inside the nucleons to explain the spectrum of emission of an atom. The main feature of effective theories is the "separation of scales". It says that " if physics takes place at a given scale, then, it should be possible to describe it without the necessity of physics at a very different scale". In particles physics, Effective Field Theory (EFT) is widely used to simplify the calculus or to investigate new physics. It consists of an expansion parameter $\delta = p/\Lambda$ such that if we perform a calculation at the order n of δ, the associated error is at n+1 and Λ a is a heavy scale. There are two types of EFT's regarding the information on the UV theory, Top-down or Bottom-up. The Lagrangian is therefore given by,

$$\mathcal{L}_{EFT} = \sum_i C_i^{UV}(\mu)\mathcal{O}_i^{IR}(\mu), \tag{11}$$

where $C_i^{UV}(\mu)$ are Wilson coefficients, $\mathcal{O}_i^{IR}(\mu)$ are operators and μ a given energy. Wilson coefficients are related to microscopic physics and consequently universals [33].

In the first type, Top-down (see Fig. 3), we know the UV theory and we "integrate out" the heavy degree of freedom to get the low-energy description. This integration out is a Taylor expansion of the propagator provided by the fact that the energy is smaller than the mass. It is used to simplify calculations, while Wilson coefficients are obtained by the UV theory. For example, we can quote the "Theory Quark Effective Theory (HEQT)" or the "Soft Collinear Effective Theory" (SCET). In the second type, Bottom-up (see Fig. 3), we don't know the UV theory. The construction of the Lagrangian is based on low-energy symmetries and relevant degrees of freedom. The values of Wilson coefficients are extracted from the experiment's data. This is the case for Standard Model Effective Fields Theory (SMEFT), that we will talk later, and Chiral Perturbation Theory (χPT) [33].

2.2.1 Fermi's theory

One interesting example of Effective Field Theory is the Fermi's theory of the weak interaction. Originally formulated to explain the beta decay of the neurton or the muon decay, it corresponds to the bottom-up approach since the underlying theory (i.e. the standard model) was not formulated and the W boson not discovered (see Fig.2a-2b),

$$n \to p + e^- + \bar{\nu}_e \qquad \text{or} \qquad \mu^- \to e^- + \bar{\nu}_e + \nu_\mu$$

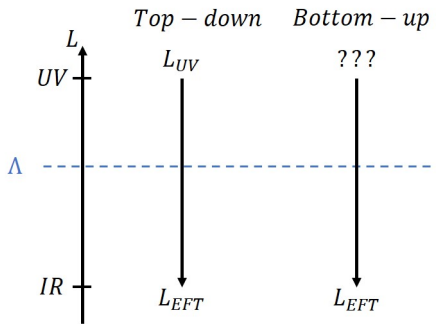

Figure 3: EFT approach, Top-down and Bottom-up

In the case of the neutron decay, the Lagrangian is composed of 4 fermions: electron, neutrino, proton and neutron, all considered as elementary,

$$\mathcal{L}_{Fermi} = -\frac{G_F}{\sqrt{2}}(\bar{\psi}_e\gamma^\mu(1-\gamma_5)\psi_\nu)(\bar{\psi}_n\gamma^\mu(1-\gamma_5)\psi_p) \tag{12}$$

Firstly, the dimensional analysis in the natural units ($\hbar = c = 1$), implies that $[G_F] = -2$, because $[\psi] = 3/2$ and $[S] = 0$. Even if we don't know the underlying theory, as soon as the constant is fixed by the experiment's data, the Fermi theory is fully predictable. Secondly, a look at the scattering of electron and neutrino, $\nu + e^- \to \nu + e^-$, tells that it growths with energy,

$$\sigma = \frac{G_F^2 S}{\pi} \tag{13}$$

with $S = E_{CM}^2$. This cross section breaks unitary and therefore informs us that the theory is not complete. The unitary requirement informs us that an underlying theory must exists before an energy of 300 GeV. In addition, UV theory is nothing but the standard model, so we can understand the principle of the Top-down approach. Indeed, in the standard model, we can compute the cross section of the above process,

$$\sigma = \frac{G_F^2 S}{\pi}\frac{1}{1+S/m_W^2} \tag{14}$$

where the behaviour at high energy is regularized, if $E >> m_W$ then $\sigma \sim \frac{G_F^2 m_W^2}{\pi}$ and at low energy we find the previous result, $\sigma \sim \frac{G_F^2 S}{\pi}$. Finally, we can proceed to the "matching procedure" to find the value of the Wilson coefficient (G_F) by integrating out the heavy degree of freedom (i.e. W boson). So we need to compute the amplitude of the process in both Fermi's theory and standard model. The Fermi's one is proportional to G_F

$$\mathcal{A}_{Fermi} \propto G_F, \tag{15}$$

while proportional to the W propagator in the standard model,

$$\mathcal{A}_{SM} \propto \frac{g_W^2}{k_W^2 - m_W^2}. \tag{16}$$

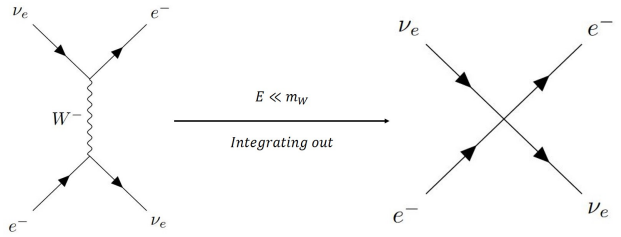

Figure 4: Neutrino scattering in SM and Fermi's theory

In the region of validity of the Fermi's theory, $E << m_W$, the two amplitude must be identical, so we find that the matching condition is

$$G_F \propto \frac{g_W^2}{m_W^2}, \tag{17}$$

where the Wilson coefficient is expressed in term of a coupling constant and the mass of the integrated out degree of freedom of the standard model. As shown in Fig. 4, the SM diagram reduces to a 4-point interaction since the momenta of the W is too small and therefore almost not propagate [28] [32] [33].

2.2.2 Standard Model Effective Field Theory

We expect that the standard model may not be valid above a few TeV so we will build an effective theory to seek the UV theory, the Standard Model Effective Field Theory (SMEFT). First we need to specify the expansion parameter and therefore demand the cut-off to at $\Lambda >> m_h$, much bigger than the weak scale. Secondly, we need to specify the matter content of the theory, which is chosen to be the same as the standard model (see Tab. 1). We also need to specify the symmetries of the theory, we assume that SMEFT is invariant under gauge group of the standard model,

$$\mathcal{G}_{SMEFT} \;=\; SU(3)_c \otimes SU(2)_L \otimes U(1)_Y$$

as well as Lorentz group. Nevertheless, we can also assume other symmetries such as baryon and lepton number conservation. Finally, we should write the most general Lagrangian that respect these symmetries,

$$\mathcal{L}_{SMEFT} = \mathcal{L}_{SM} + \sum_{d>4} \sum_{i=1}^{N_d} \frac{c_i^{(d)}}{\Lambda^{d-4}} \mathcal{O}_i^{(d)}, \tag{18}$$

where c_i are the Wilson coefficient and $\mathcal{O}_i$ operators of SM fields. Operators have the following expression,

$$\mathcal{O}_i \sim (\psi\bar{\psi})^{N_\psi} D^{N_D} F^{N_F} \phi^{N_\phi}, \tag{19}$$

where ψ are spinors, D derivatives, F fields strength tensors and ϕ scalars. For example, in dimension-six,

$$[\mathcal{O}_i] = \frac{3}{2} N_\psi + 2N_F + N_D + N_\phi = 6. \tag{20}$$

So there are only 3 types of operators, purely bosonic (X^3, H^6, H^4D^2, H^2X^2), mixed (ψ^2H^3, ψ^2XH, ψ^2H^2D) and purely fermionic (ψ^4). Note that X is related to F and H related to ϕ. The total number of operators increases quickly with the number of dimensions. For example, there are 2499 operators of dimension-six.

Finally, whereas the SMEFT only contains dimension-six operators, the cross section take the following expression,

$$\sigma_{tot} = \sigma_{SM} + \sum_{i=1}^{N_{op}} \frac{c_i}{\Lambda^2}\sigma_i + \sum_{i=1}^{N_{op}}\sum_{j=1}^{N_{op}} \frac{c_i c_j}{\Lambda^4}\sigma_{i,j}, \tag{21}$$

where the σ_i are interferences between SM and dimension-six operators and $\sigma_{i,j}$ are the contribution of product of operators. Phenomenologically, the main contribution arises at Λ^{-2} if the interference term is nonzero and is linear in the Wilson coefficient.

2.3 W Boson

2.3.1 W boson in the standard model

The W boson was postulated by Glashow, Salam and Weinberg in electroweak unification theory formulated in the 1960s. This theory predicted the existence of three massive gauge fields as mediators of the weak interaction, $W^{\pm}$ and Z^0. These particles were discovered at CERN by UA1 and UA2 experiments. Indeed, in 1983, experiments were conducted under the supervision of Carlo Rubbia and Simon Van der Meer at the "Super Proton–Antiproton Synchrotron" (SppS) and led to the measurement of these masses.

In addition the W boson is unstable, its world average width is $\Gamma_W = 2.091 \pm 0.001\, GeV$ [30], its lifetime is $\tau \sim 10^{-25} s$. It means that we cannot directly observe a W boson in the detector. We then need to look at its decay channel by summing particles' energy. In the case of the W, the preferred channel is $p\bar{p} \to W^+ \to l^+ \nu$ and $p\bar{p} \to W^- \to l^- \bar{\nu}$. Because of neutrinos that are not observed in the detectors due to their very weak interaction, we need to reconstruct the quadri-vector of all observed particles. Then we sum up for momenta of each particle, if we have detected all of them, this sum should be equal to zero. If not, the missing quantity is related to missing energy. We should also note that, depending on the collision nature, the production of W^+ and W^- could be different. For example, at SppS or at Tevatron, the collision is proton/antiproton and therefore there is no difference between W's. At the LHC, the collision is proton/proton, so the production of W^+ is enhanced.

The standard model value of the W-mass is fixed by analytical combination of, on one hand, a set of high-precision experimental data (m_Z, m_H, m_t, α_{EM} and muon's lifetime), and on the other hand, higher order correction in the perturbative expansion,

$$m_W^2\left(1 - \frac{m_W^2}{m_Z^2}\right) = \frac{\pi \alpha_{EM}}{\sqrt{2} G_F}(1 + \Delta r), \tag{22}$$

where Δr are radiative corrections within SM and its extension [12]. For the SM, this term depends on the Higgs and top mass. The standard model contribution to these radiative corrections are mostly releted to the Higgs mass and the top mass. In some extension of the standard model, it could depend on new particles and interactions. Consequently, the W-Boson mass prediction is really sensitive to Beyond Standard Model (BSM) physics. The SM value is $m_W = 80.357 \pm 0.006\, GeV$ (see Fig.6). Combining measurements from Tevatron and LHC, the world average is given by $m_W = 80.379 \pm 0.012\, GeV$ [26].

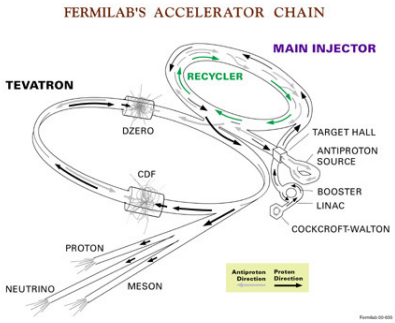

Figure 5: Tevatron acceleration chain [25]

2.3.2 CDF II results

The Tevatron was a synchrotron particle accelerator at Fermilab in Illinois. It was accelerating proton and antiprotons at 99.999954 % of the speed of light. It finished its activities in 2011. Before that is was the second most powerful accelerator after the LHC at CERN, by reaching an $\sqrt{S} = 1.96\,TeV$. Just like at CERN, a serie of accelerators was used to reach the desired energy (see Fig.5). First, negative hydrogen ions were produced and sent in a linear accelerator (LINAC) to reach 400 MeV. Then, they passed through carbon foil to remove their electrons. Protons produced were accelerated by the "booster" to an energy of 8 GeV. Then they were stored in the "Main injector". Some of these protons were used to produce antiprotons by colliding with a nickel target. Antiprotons were harvested and sent to the main injector that was accelerating both protons and antiprotons and injecting them in the Tevatron. The latter had two detector, CDF (Collider Detector at Fermilab) and D0. It has been used for example to detect for the first time the production of a top quark [25].

On 8 April 2022, the CDF collaboration published, in Science, a paper (see Ref. [26]) where they have measured a mass for the W in tension with the SM prediction (7 sigmas), as shown in the Fig. 6. Indeed they measured a mass of $m_W = 80.4334 \pm 0.0094\ GeV$ from a sample of 4 million W candidates. To fit the data gained by the experiment, they generated a template with Monte Carlos (MC) method for different m_W and different observables. These distributions are just standard model distributions with different W masses. Then they fit this template with the sample's distribution.

2.3.3 W boson as a gate to new physics

A W-mass shift could be a probe of new physics. For example, it could be the sign that the Higgs is a composite particle of the existence of a "dark photon" [26]. On one hand, many have investigated an SMEFT approach by looking at operators that gives an positive mass shift. However, on the other hand, one can also consider a SMEFT approach but without modifying the mass of the W itself.

Indeed, if we consider the following effective operator,

$$\mathcal{O}_{lq}^{(3)} = (l_p \gamma_\mu \tau^I l_r)(q_s \gamma^\mu \tau^I q_t), \tag{23}$$

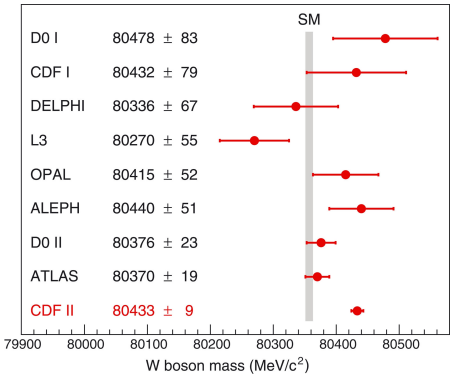

Figure 6: Comparison of SM value alongside measured m_W

where l and q are fermions and quarks, respectively, τ^I are Pauli matrices. This operator contribute to the production of the neutrinos and leptons that are used to measure the m_W (see Fig. 7). Consequently, the Lagrangian has now the following expression,

$$\mathcal{L}_{SMEFT} = \mathcal{L}_{SM} + \frac{C_{lq}^{(3)}}{\Lambda^2}\mathcal{O}_{lq}^{(3)}. \tag{24}$$

From the section 2.2.2, we can write the total cross section for this model,

$$\sigma_{tot} = \sigma_{SM} + \frac{C_{lq}^{(3)}}{\Lambda^2}\sigma_{lq} + \frac{(C_{lq}^{(3)})^2}{\Lambda^4}\sigma_{lq}^2, \tag{25}$$

This cross-section has the interference as next leading contribution (Λ^{-2}), if nonzero. This means that it will modify the shape of the distributions themselves. Also, if we neglect the term in Λ^4, the contribution of new physics is linear in the Wilson coefficient.

Therefore, the new physics modify the distributions used to fit the mass of the W-boson. The idea of the work is to investigate the effect of this 4-fermion operator on the shape of distributions and its implication in a mass fit. Indeed, if the W boson is heavier than expected, the distributions should be mostly shifted to the right. But if the Wilson coefficient is nonzero, could this modification be interpreted as a mass shift while the mass of the W remains unchanged ? If possible, what would be the required value of the Wilson coefficient to get the mass shift obtained by the CDF II collaboration ?

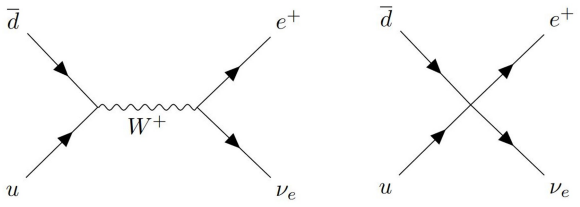

Figure 7: Example of diagrams SM (left) and SMEFT (right)

3 Methodology

In this section, we describe the methodology followed during this work. First, we show how we built the model expanding the standard model with the four-fermion operator. Second, we describe the generation of distributions of standard model and new physics. Finally, we talk about the fitting strategy.

3.1 Model construction

The model is built with the package for Mathematica [37], Feynrules [2] [10]. This allows us to compute the Feynman rules of our model. First we need to specify the parameters. In addition to those present in the standard model, we introduce two new parameters: the Wilson coefficient called $C_{lq}^{(3)}$ and the scale of new physics, Λ, set to 1 TeV. The Lagrangian considered is defined by Eq.24. We apply the *massless* restriction where all fermion's mass is set to zero except for the bottom quark, top quark and tau lepton. We finally export this model in UFO to be used in Madgraph [3].

We can also check that the model is working properly inside Madgraph by generating its interference with the standard model. It corresponds to the second term of Eq.25 and so it is proportional to the Wilson coefficient. We have computed the cross section of the process. We have checked that the interference vary linearly with the Wilson coefficient for a few values.

3.2 Distributions

3.2.1 Standard Model

In this section, we develop the procedure to generate the standard model distributions. Following [1], we want to plot transverse momentum (p_T^l) and transverse mass (m_T) distributions for both electrons and muons as well as transverse momentum for the missing energy (p_T^ν). We use madgraph to generate the following processes, $p\bar{p} \to l^+ \nu$ and $p\bar{p} \to l^- \bar{\nu}$ [3].
We generate events at leading order with only one jet and the pdf set "nn23lo1" (with $C_{lq}^{(3)} = 0$). Since the W-mass is an internal parameter in Madgraph, its value is fixed by m_Z, α_{EM} and G_F in Tab.2. With these parameters, the W-mass is 80 418.23 MeV, and will be the value for this analysis. In Table 3, one can find the cuts for all runs performed in this section.

Parameter inside Madgraph	*Values*
m_Z	91.18760 GeV
α_{EM}	$(132.0570)^{-1}$
G_F	1.166370×10^{-5} GeV^{-2}
α_s	1.18400×10^{-1}
Γ_W	2.0850000 GeV

Table 2: Table of parameters inside Madgraph

In order to lower the impact of the numerical noise, we generate 20 runs and average over it. The average is given by,

Description of the cuts	*Values*
Minimum jet's p_T	20 GeV
Minimum lepton's p_T	10 GeV
Minimum missing energy	0 GeV
Maximum jet's rapidity	5.0
Maximum charged lepton's rapidity	2.5
Minimum charged lepton's rapidity	0.0
Minimum distace between jet and lepton (drjl)	0.4 GeV^{-1}
Minimum invariant mass for all leptons	0.0 GeV

Table 3: Table of cuts for the runs

$$\mu(i) = \frac{1}{N}\sum_{l=1}^{N} y(i)_l, \tag{26}$$

where i stands for the index over bins and $y(i)_l$ is value of the bin for the l^{th} distribution averaged. The numerical noise is quantified by the standard deviation,

$$S^2(i) = \frac{1}{N-1}\sum_{l=1}^{N}(y(i)_l - \mu(i))^2. \tag{27}$$

We present these distributions at parton level (see Fig.8a, 8c and 8e) displayed with Madanalysis 5 with the following expression [19],

$$p_T = \sqrt{p_x^2 + p_y^2} \tag{28}$$

$$m_T = (\sum \vec{E}_T)^2 - (\sum \vec{p}_T)^2 \tag{29}$$

The bounds of the plots are chosen following [1]. These are characterized by a quick increasing slope and then a sharp edge around 40 GeV and 80 GeV for transverse momentum and transverse mass respectively. After that, we perform the parton shower with Pythia 8 [34]. We are a bit more restrictive with the cuts applied during the plots. Indeed, we select all $p_T > 30\ GeV$ and all $\mid \eta \mid < 1$, where η is the pseudo-rapidity. As shown on Fig.8b, 8d and 8f, on one hand, we find that the transverse momentum distribution is close to ones shown in [1] and [26]. On the other hand, the transverse mass distribution is modified compared to the parton level but is still different from what we are expecting. These distributions are slightly increasing to the maximum like expected but the peak is too big and the right edge too sharp. This difference can be partially explained by the definition of the missing transverse energy of Madanalysis. It corresponds to every neutrino produced during the process. Since we have not performed a detector simulation, some missed energy might no be taken into account. For example, if a particle with very small momentum is emitted, it will spin along the beam direction.

3.2.2 New Physics

In this section, we describe the methodology to generate SMEFT distributions. We are following the same steps as in section 3.2.1 (cuts, parameter value, pdf, ...) but with non-zero values of $C_{lq}^{(3)}$.

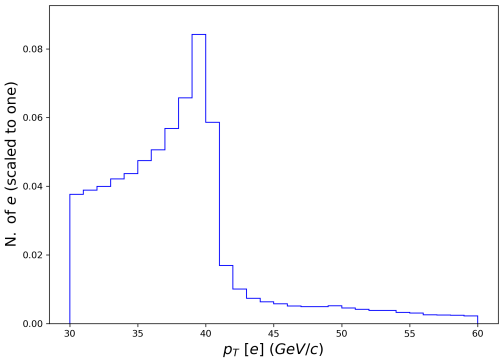

(a) p_T electronic at parton level

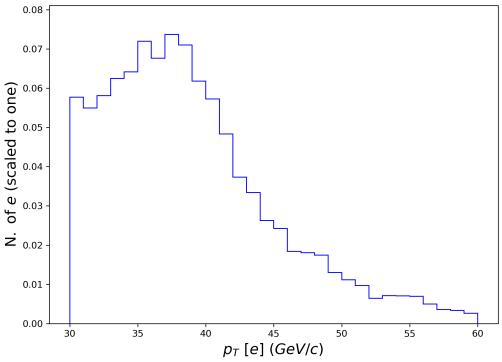

(b) p_T electronic at hadron level

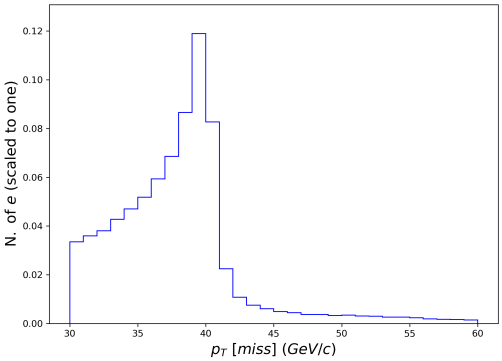

(c) p_T of missing energy at parton level

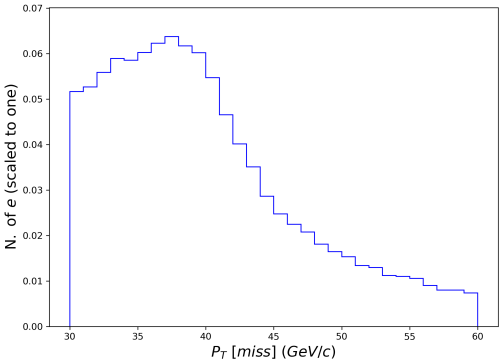

(d) p_T of missing energy at hadron level

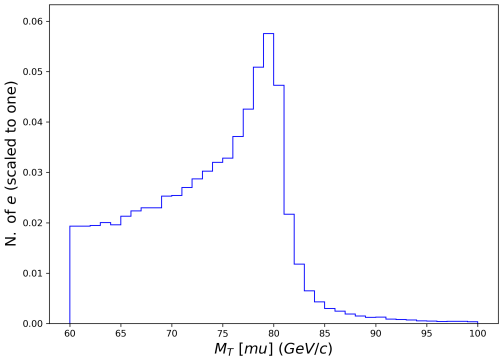

(e) m_T muonic at parton level

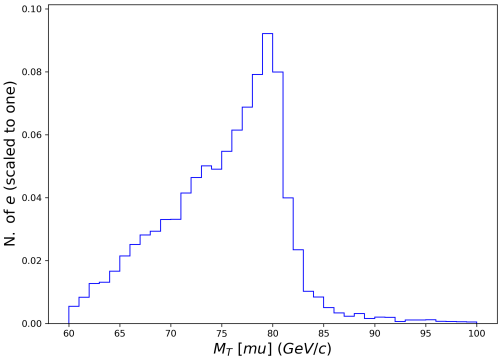

(f) m_T muonic at hadron level

Figure 8: Standard model distributions of transverse momentum (p_T) and transverse mass (m_T)

m_W (GeV)	α_{EM}		
79.4	124.921	80.6	134.026
79.6	126.292	80.7	134.890
79.8	127.717	80.8	135.773
80.0	129.199	80.9	136.675
80.1	129.963	81.0	137.596
80.2	130.743	81.1	138.537
80.3	131.539	81.3	139.498
80.4	132.351	81.4	141.486
80.5	133.180	81.6	143.564

Table 4: Structure fine constant for various m_W

A closer look at the distributions, when $C_{lq}^{(3)}$ is increasing, shows an important contribution at the tails from third term of Eq.25. Hence, when we renormalize to unity the distributions, to compare them, ones with higher $C_{lq}^{(3)}$ will be shifted to lower values. This is shown on Fig.9a-9f for curves on red or on blue. This causes problems when we perform the fit. Therefore, we apply restrictive cuts on distributions by choosing $p_T < 60\,GeV$ for all particles. We can note that similar restrictions have been chosen in [1] and [26]. Indeed, the following cuts were applied to obtain their "high purity sample" $30 < p_T < 55\,GeV$ for electrons, muons and missing energy as well as $60 < m_T < 100\,GeV$ for the transverse mass.

3.3 Fitting strategy

In this section, we describe the fitting strategy used. We want to generate a "template", in other words, a set of distributions for different observables (m_T, p_T^l and p_T^ν) with different masses of W. Since the W-mass is an internal parameter in Madgraph with the following expression,

$$m_W = \sqrt{\frac{m_Z^2}{2} + \sqrt{\frac{m_Z^4}{4} + \frac{\alpha_{EM}\pi m_Z^2}{G_F\sqrt{2}}}}, \tag{30}$$

where m_Z is the Z boson mass, α_{EM} is the fine-structure constant and G_F the Fermi's constant. To modify m_W we should modify one of these quantities. For example if we modify m_Z, we will modify θ_W because $cos(\theta_W) = \frac{m_W}{m_Z}$ and the coupling constant $g_1 cos(\theta_W) = g_2 sin(\theta_W) = e$ and therefore we will modify the interaction between the W boson and fermions,

$$\begin{cases} \mathcal{L}_{W-Leptons} = -\frac{g_2}{\sqrt{2}}[\bar{\nu}\gamma^\mu(1-\gamma_5)eW_\mu^+ + \bar{e}\gamma^\mu(1-\gamma_5)\nu W_\mu^-] \\ \mathcal{L}_{W-Quarks} = -\frac{g_2}{\sqrt{2}}[\bar{u}\gamma^\mu(1-\gamma_5)dW_\mu^+ + \bar{d}\gamma^\mu(1-\gamma_5)uW_\mu^-] \end{cases}.$$

In addition, if we modify α_{EM} we are also modifying e since $\alpha = \frac{e^2}{4\pi}$ in natural units. However, it will only change globally the distributions, so if we normalize all distributions to unity, it will not contribute. Hence we choose to modify α_{EM} to modify the W-mass (see Table 4) and are obtained by inverting the equation (30) with Mathematica. The distributions are plotted with Madanalysis for the cuts mentioned before.

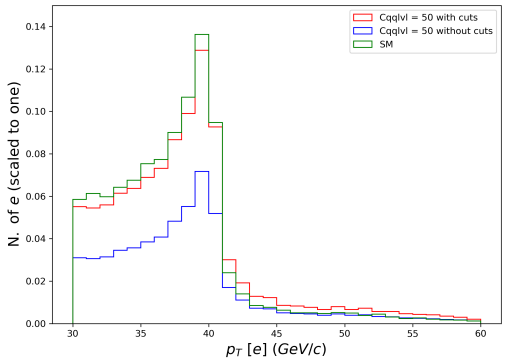

(a) p_T electronic at parton level

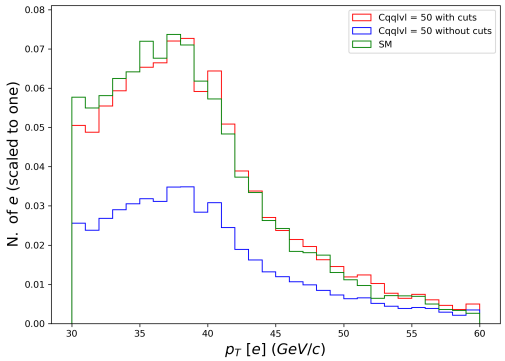

(b) p_T electronic at hadron level

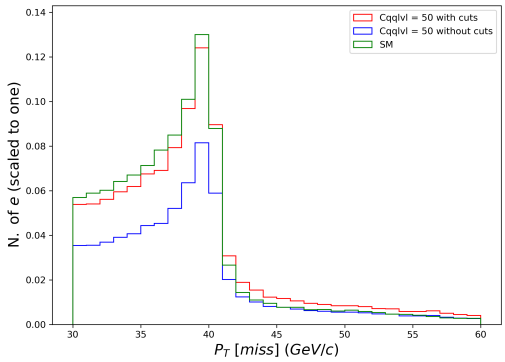

(c) p_T of missing energy at parton level

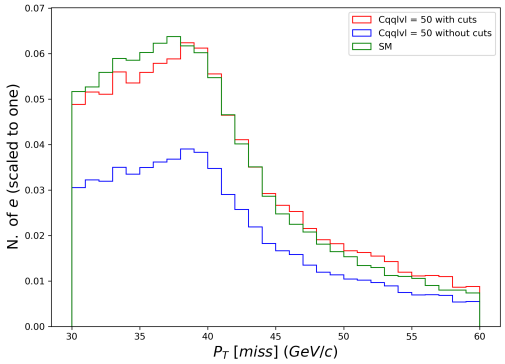

(d) p_T at hadron level

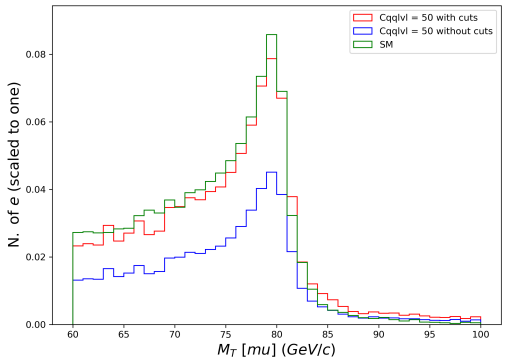

(e) m_T muonic at parton level

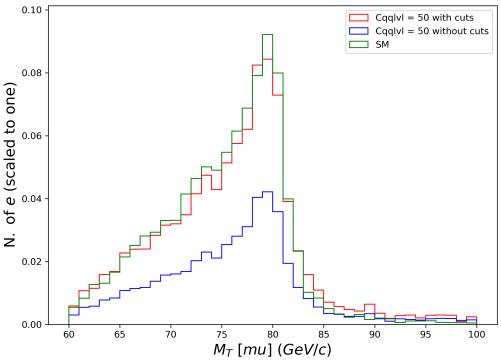

(f) m_T muonic at hadron level

Figure 9: Standard model and new physics distributions of transverse momentum (p_T) and transverse mass (m_T)

The fit is performed by calculating χ^2 for masses in the Table 4 for $32 < p_T < 48\,GeV$ and $65 < m_T < 90\,GeV$,

$$\chi^2_{n-1} \sim \sum_{i=1}^{n} \left(\frac{x(i) - \mu(i)}{\sqrt{\frac{S_x^2}{N_x} + \frac{S_\mu^2}{N_\mu}}} \right)^2 , \tag{31}$$

where n is the number of bins fitted, N_x and N_μ the number of distributions averaged, S_x and S_μ the sample variance and x and μ the bins' value of interest and of template distributions respectively. Then, we fit the χ^2 obtained by a parabola where the minimum gives the best fitted mass ($\hat{m}_W$) and the 1-sigma confidence intervals by $\chi^2(\hat{m}_W \pm \sigma_{\hat{m}_W}) = \chi^2_{min} + 1$ [6]. This is valid in the Gaussian limit and with only one parameter fitted. In addition, we will use another method to compute confidence intervals. They are defined to be the abscissa of the intersection between the fitted curve and the value of the χ^2 Cumulative Distribution Function for a given confidence level. We also shall discuss the degree of freedom. Strictly speaking, if we were fitting on every bin it should be $n-2$ since the distributions are normalized to unity. Nevertheless, we are not fitting on all bins so we are between $n-1$ and $n-2$. We choose $n-1$ because it corresponds to the most conservative option. Indeed, for the second method, the number of degrees of freedom will be bigger than in the first method and so will be the confidence intervals. We also compute the R^2 to quantify the quality of the parabolic fit,

$$R^2 = 1 - \frac{\sum_{i=1}^{n}(y_i - \hat{y}_i)^2}{\sum_{i=1}^{n}(y_i - \bar{y})^2}, \tag{32}$$

where the y_i is the ith fitted quantity, $\hat{y}_i$ is the predicted value by the fit and $\bar{y}$ the mean of fitted quantities. On plots are given the χ^2_{min}, the related fitted mass, the associated mass uncertainty (at 1 sigma) and the R^2.

Finally, to verify its quality, we perform a fit with SM distributions at the theoretical W-mass of $80.418\,GeV$. We use the first method to compute the confidence intervals. On Fig.10a-10b, we present first a fit of distribution at parton level. We can see that the best fitted mass and its confidence interval at 5-sigmas contains the theoretical mass cited above. However, we note that the theoretical mass is contained within the 1-sigma interval for m_T^μ and 3-sigma for p_T^e. Moreover, if $\chi^2/dof \sim 1$ the fit is considered as good while if $\chi^2/dof >> 1$ is considered as bad. Here the $\chi^2/dof \sim 1$, which means that the fit is good and we can trust its results. If we check it also at hadron level, we can see that it works for the two transverse masses, muonic (see Fig.10d) and electronic, but not for transverse momentum (see Fig.10c). Therefore, we will focus the analysis on the transverse momentum and transverse mass at parton level and only transverse mass at hadron level.
We also show at parton and hadron level the second method to compute the confidence intervals (see Fig.10e). In this case, the 1-sigma confidence interval is 3 times bigger than the previous method but depends on the quality of the fit (χ^2_{min}) and the shape of the parabola.

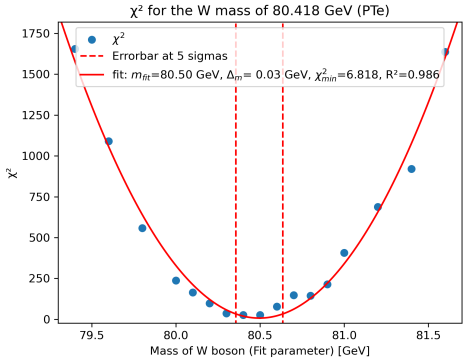

(a) p_T^e at parton level

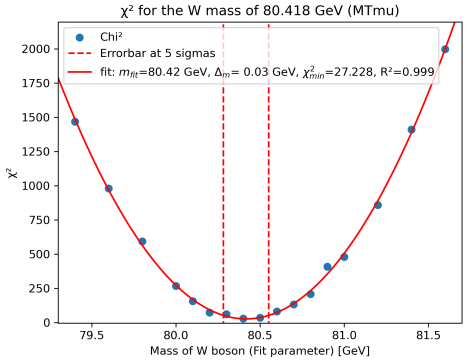

(b) m_T^μ at parton level

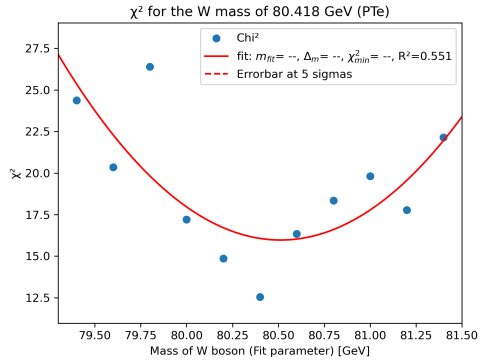

(c) p_T^e at hadron level

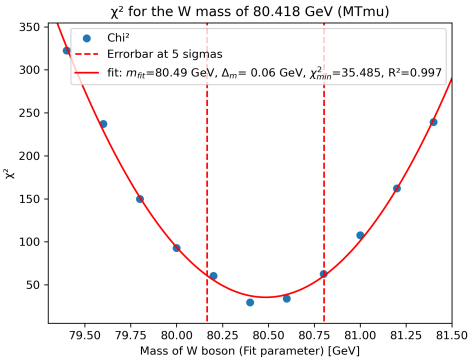

(d) m_T^μ at hadron level

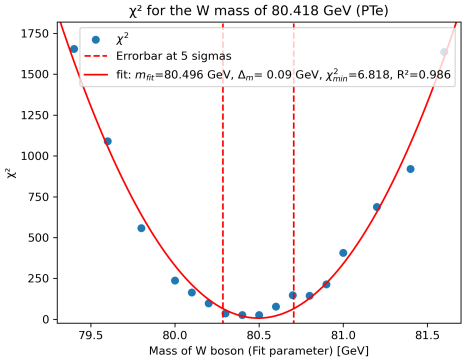

(e) p_T^e at parton level

Figure 10: Plotted χ^2 for each mass and the fitted parabola for p_T^e and m_T^μ at parton and hadron level

4 Results and Discussion

In this section, we present results of the fits at both partonic and hadronic level. We will discuss the possible mass shift depending on the Wilson coefficient. We restrict the analysis to a model linear in $C_{lq}^{(3)}$. The idea is to extrapolate its value to find the mass deviation observed at the CDF II collaboration. In addition, we will discuss the impact of this new physics on the parameters that determine the mass of the W-mass in the standard model. Finally, then we will discuss the different constraints on this coefficient.

4.1 Parton Level

In this section, we present and discuss the results at parton level for 10 000 events per run. Here we neglect the term on Λ^{-4}, to be linear in the Wilson coefficient. First, we generate distributions for different values of the Wilson coefficient and we perform a fit. On Fig.11a-11f, we have the results of 6 fits for $C_{lq}^{(3)}$ equal to -10, 10, -20, 20 and -40, 40 respectively. This fit gives the best fitted mass and the 5-sigma confidence interval associated. We can see that, with the p_T^e as an example, the minimum of the χ^2 is being shifted to the right for positives Wilson coefficients (see Fig.11b, 11d and 11f) and shifted to the left for negative values (see Fig.11a, 11c and 11e). It means that to have a positive shift W-mass in accord to the CDF II results we need to take a positive value of the Wilson coefficient. Then we observe that for $C_{lq}^{(3)} = 40$, the mass shift obtained by the fit excludes the theoretical value of the W-Boson mass, $80.418\ GeV$. So we have shown that the new physics contribution can deceive a mass fit and gives a new mass to the W-boson while its value is not changed in the model. It is the modification of the distributions' shape that are interpreted by the fit as a mass shift.

We also observe, on Fig.11, that the χ^2_{min}/dof is increasing. This is also shown on Fig.12a-12b, where we have plotted the χ^2_{min}/dof for different values of $C_{lq}^{(3)}$ for p_T^e and m_T^μ. On these figures we have fitted the points with a parabola and computed the R^2 factor. As we can see, the R^2 are close to one so it means that the evolution of $C_{lq}^{(3)}$ follows a χ^2 law. Hence as much as the Wilson coefficient increases, the further we are from the SM hypothesis. This really shows that the contribution of new physics is not a "simple" mass shift but a complete modification of the distributions' shape. Nevertheless, the χ^2_{min} should also have followed a global χ^2 law in the case of a simple mass shift. To illustrate thist two cases, one can plot on Fig.15, the difference between NP distribution and SM model distribution at $m_W = 80.418\ GeV$ (see Fig.15a and 15c) and between SM at the best fitted mass and SM model $m_W = 80.418\ GeV$ (see Fig.15b and 15d). As we can see, the shapes of these distributions are totally different where, if it was just a mass shift, it should be roughly the same. Another argument is developed by computing the confidence intervals with the second method explained in the "methodology" section. As shown on Fig.14a, we can see that the confidence interval computed at 5-sigma has decreased compared to Fig.10e. We also note that the 1-sigma interval is no longer computable because χ^2_{min} is bigger than χ^2 Cumulative Distribution Function at 1-sigma. For $C_{lq}^{(3)} = 30$, it is not possible to compute the 5-sigma confidence interval (see Fig.14b). This witnesses that the template distributions and NP distributions are not generated under the same hypothesis. Moreover, we can see on Fig.12a-12b that for values of $C_{lq}^{(3)}$ bigger, in absolute value, than 50 we cannot longer really trust the fit, because $\chi^2_{min}/dof >> 1$. This condition is less restrictive than the one coming from the second method.

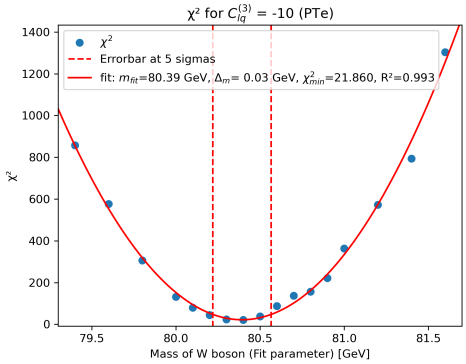

(a) χ^2 for $C_{lq}^{(3)} = -10$

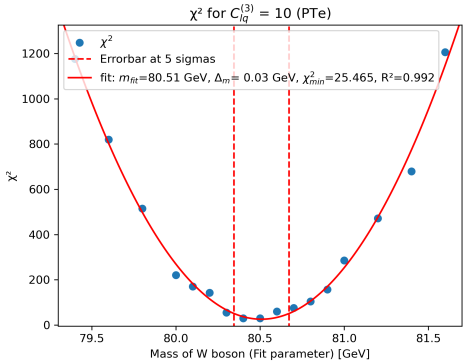

(b) χ^2 for $C_{lq}^{(3)} = 10$

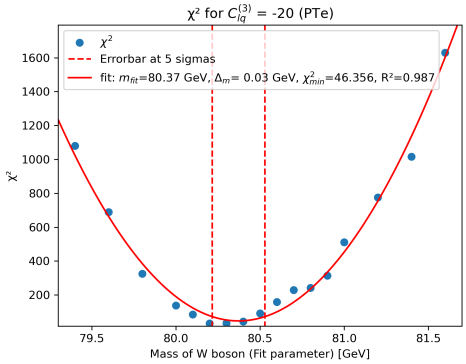

(c) χ^2 for $C_{lq}^{(3)} = -20$

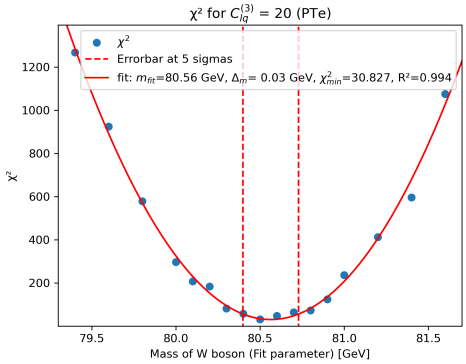

(d) χ^2 for $C_{lq}^{(3)} = 20$

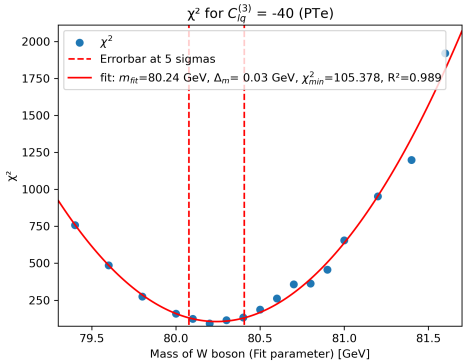

(e) χ^2 for $C_{lq}^{(3)} = -40$

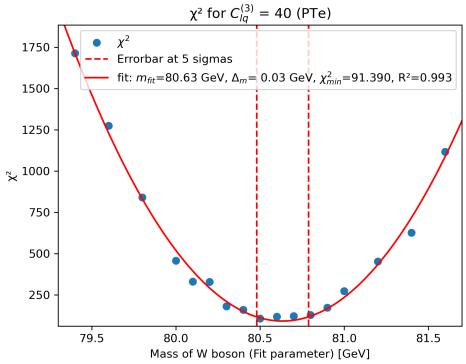

(f) χ^2 for $C_{lq}^{(3)} = 40$

Figure 11: Evolution of the $\chi^2(m_W)$ and the fitted parabola for increasing values of $C_{lq}^{(3)}$ at parton level

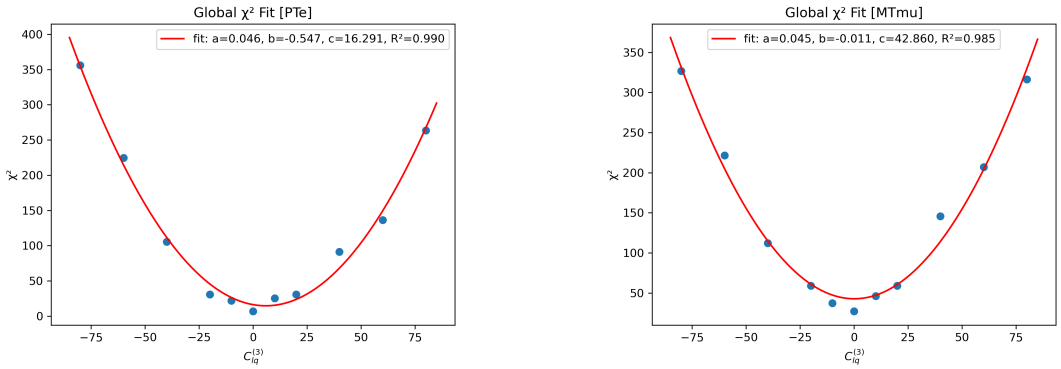

(a) χ^2_{min} for p_T^e (b) χ^2_{min} for m_T^μ

Figure 12: Evolution of the χ^2_{min} for increasing values of $C_{lq}^{(3)}$ at parton level

In other to extrapolate the value of the Wilson coefficient that would be needed to get the mass shift observed by the CDF II collaboration, we have restricted the analysis to a model linear in $C_{lq}^{(3)}$. We need to verify the linearity of the mass deviation fitted (m_{Fit}) in terms of the Wilson coefficient,

$$deviation(\%) = \frac{(m_{Fit} - 80.418)}{80.418} * 100. \tag{33}$$

On Fig.13, one can find the deviation to the theoretical W-mass in function of the Wilson coefficient and their confidence intervals. We can see that the linearity is valid up to 3-sigma for all distributions. The only value of $C_{lq}^{(3)} = -100$ that is not crossing the fitted curve within 3-sigma is the transverse momentum for the missing energy (see Fig.13b). It corresponds to a value of the Wilson coefficient that is bigger, in absolute value, than 60 and where the results of the fit should be considered with caution.

We have also performed this analysis at parton level with runs of 100 000 events. This allowed us to reduce the numerical noise by roughly a factor 3 (see Tab.5). In this table, we have computed the average standard deviation over bins and over the distributions of the template and the new physics distributions. One can find that the needed Wilson coefficient to exclude at five sigmas the theoretical W-mass is $C_{lq}^{(3)} = 15$. We also observed the increase of the χ^2_{min}/dof with respect to $C_{lq}^{(3)}$. And finally, we have computed the deviation to the theoretical W-mass for the five observables and the slope of the fitted lines (see Tab.6).

4.2 Hadron Level

In this section we present the results of the fit for different values of the Wilson coefficient at the hadron level. Again, we stay linear in the Wilson coefficient. We focus on the two transverse masses since the fit for the transverse momentum is not working properly. As we can see on Fig.16, the χ^2 fitted parabola is shifting to the right while $C_{lq}^{(3)}$ is increasing. Nevertheless, the numerical noise is bigger so the confidence intervals are wider. Consequently, the theoretical W-mass is now excluded from the 5-sigma interval for $C_{lq}^{(3)} = 60$ while it was for $C_{lq}^{(3)} = 40$ at the parton level.

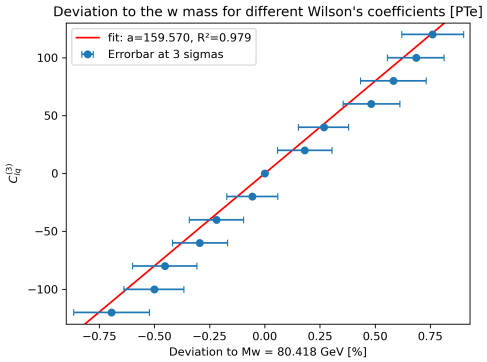

(a) Deviation for p_T^e

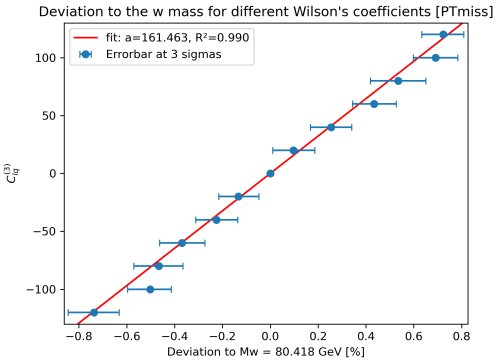

(b) Deviation for p_T^{miss}

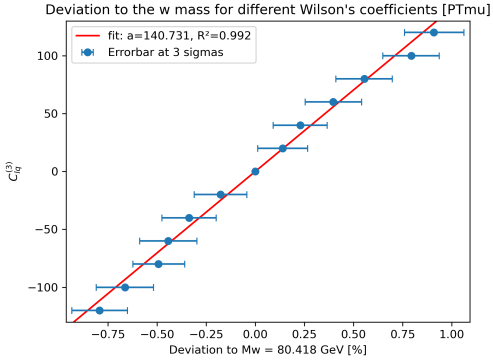

(c) Deviation for m_T^μ

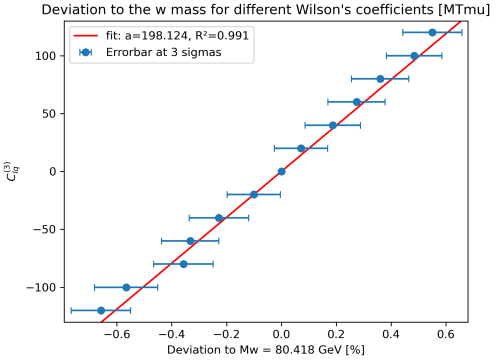

(d) Deviation for m_T^μ

Figure 13: Computed mass deviation for increasing values of $C_{lq}^{(3)}$ at parton level

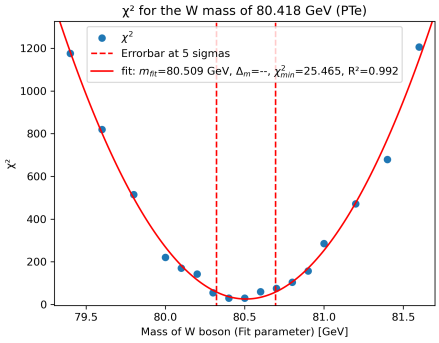

(a) χ^2 for $C_{lq}^{(3)} = 10$

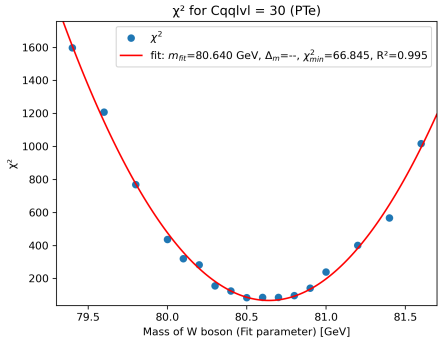

(b) χ^2 for $C_{lq}^{(3)} = 30$

Figure 14: Evolution of the $\chi^2(m_W)$ and the fitted parabola for increasing values of $C_{lq}^{(3)}$ at parton level for the second method

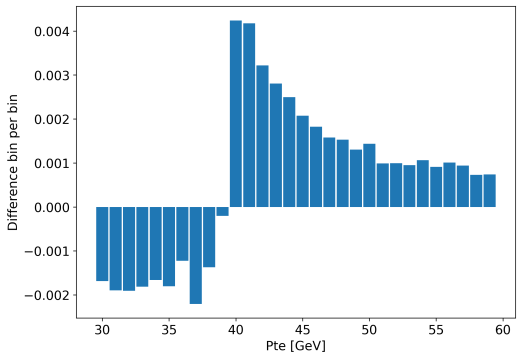

(a) NP($C_{lq}^{(3)} = 60$) vs SM(80.418 GeV) at parton level [p_T^e]

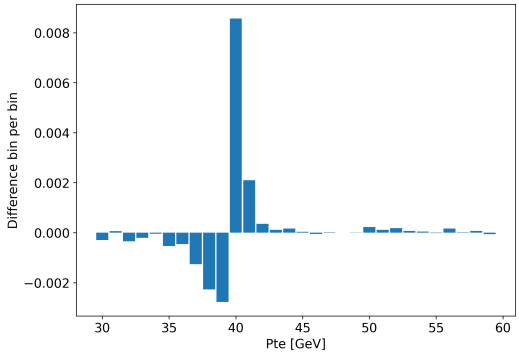

(b) SM(80.418 GeV) vs SM(m_{Fit}) at parton level [p_T^e]

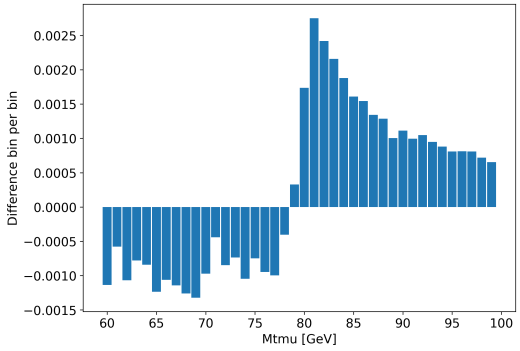

(c) NP($C_{lq}^{(3)} = 60$) vs SM(80.418 GeV) at parton level [m_T^μ]

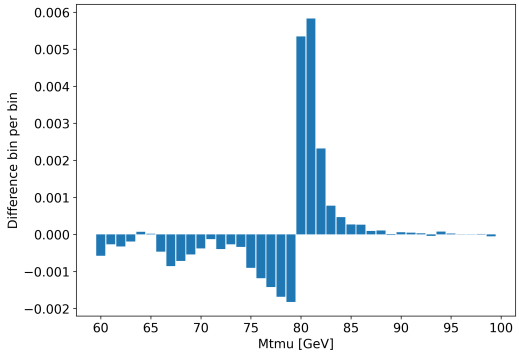

(d) SM(80.418 GeV) vs SM(m_{Fit}) at parton level [m_T^μ]

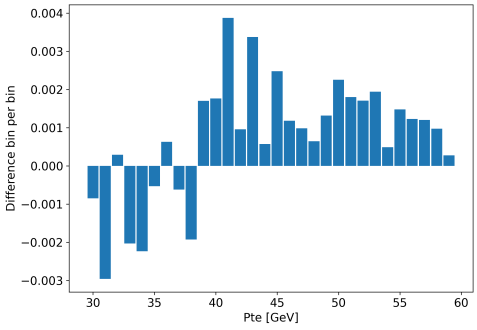

(e) NP($C_{lq}^{(3)} = 80$) vs SM(80.418 GeV) at hadron level [p_T^e]

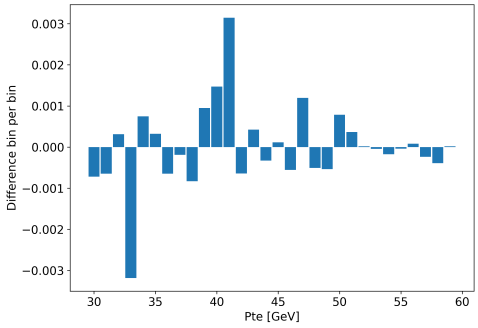

(f) SM(80.418 GeV) vs SM(m_{Fit}) at hadron level [p_T^e]

Figure 15: Difference between SM distribution at $m_W = 80.418\,GeV$ and NP distribution (left) and SM distributions at m_{Fit} (right)

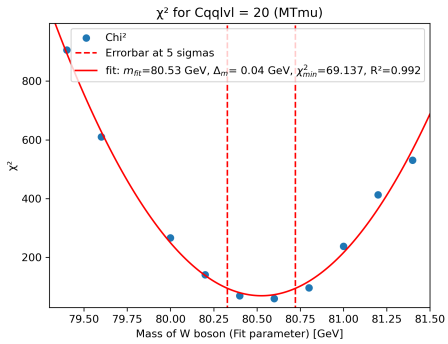

(a) χ^2 for $C_{lq}^{(3)} = 20$

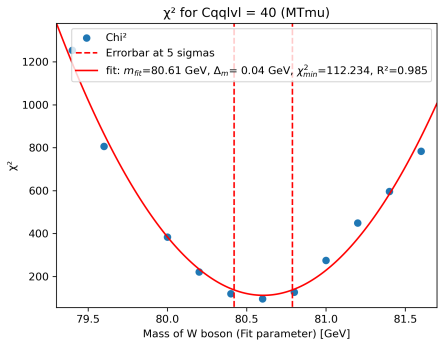

(b) χ^2 for $C_{lq}^{(3)} = 40$

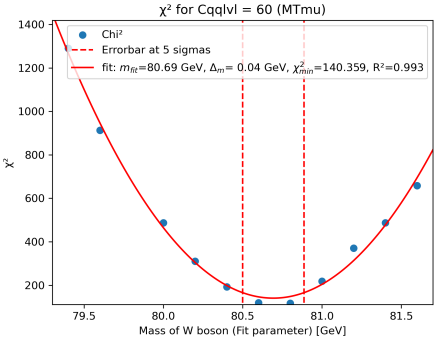

(c) χ^2 for $C_{lq}^{(3)} = 60$

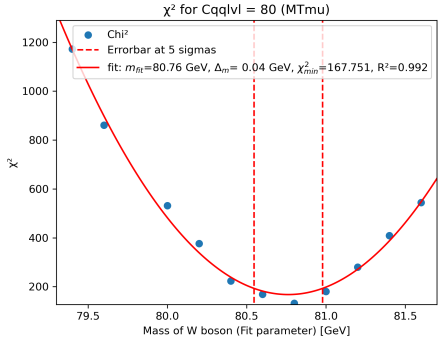

(d) χ^2 for $C_{lq}^{(3)} = 80$

Figure 16: Evolution of the $\chi^2(m_W)$ and the fitted parabola for increasing values of $C_{lq}^{(3)}$ at hadron level

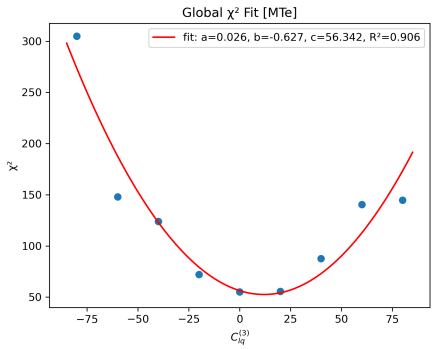

(a) χ^2_{min} for m_T^e

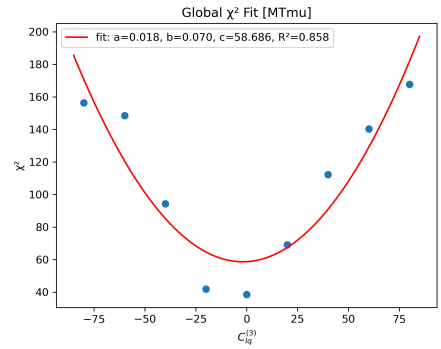

(b) χ^2_{min} for m_T^μ

Figure 17: Evolution of the χ^2_{min} for increasing values of $C_{lq}^{(3)}$ at hadron level

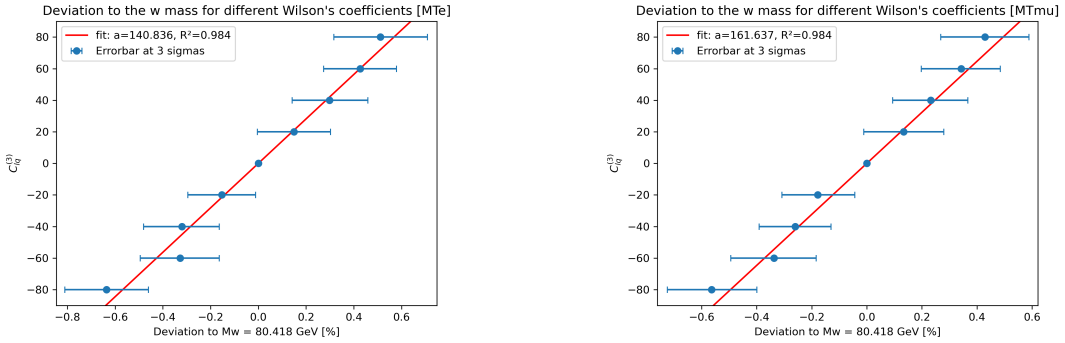

(a) Deviation for p_T^e

(b) Deviation for m_T^μ

Figure 18: Computed mass deviation for increasing values of $C_{lq}^{(3)}$ at hadron level

Observables	Numerical noise at parton level (10 000 events)	Numerical noise at parton level (100 000 events)	Numerical noise at hadron level (10 000 events)
p_T^e	0.0413	0.0131	0.0522
p_T^ν	0.0399	0.0123	0.0446
m_T^e	0.0441	0.0136	0.0508
p_T^μ	0.0440	0.0134	0.0508
m_T^μ	0.0460	0.0141	0.0530

Table 5: Table of standard deviation averaged over bins and the distributions with different mass

Similarly than at parton level, we also observe an increase of the χ^2_{min}/dof which tells us that we are further and further from the standard model hypothesis. When the $C_{lq}^{(3)} > |60|$, the results of the fit should be taken with caution. In addition, R^2 further from one than at parton level informs us that the fit is less effective. Especially for the muonic transverse mass that is just at the limit of what is usually assumed to be a good fit, $R^2 > 0.85$. This is mostly due to the numerical noise that has increased for the hadron level (see Tab.5) combined with the slowest variation of these distributions. On Fig.15e-15f, we show SM vs NP and SM vs SM at hadron level. The difference is less marked due to bigger fluctuations compared to parton level. The transverse mass is not shown because it is very similar to the parton level case. We also observe on Fig.15f that there is not the clear shape of the parton level for the case SM vs SM. This may be a part of the explanation of the impossibility to fit the transverse momentum distributions at hadron level. Since the distributions at hadron level are barely distinguishable, the fit is not working properly.

Moreover, one can check the linearity of the mass deviation in the Wilson coefficient. The graph of the deviation, computed with Eq.33, shows a linear progression with respect to $C_{lq}^{(3)}$. The fitted lines have a R^2 close to 1. Note that, like at parton level, we need to go to the 5-sigma confidence interval.

Observables	Slope at parton level (10 000 events)	Slope at parton level (100 000 events)	Slope at hadron level (10 000 events)
p_T^e	149.043	174.835	-
p_T^ν	157.022	162.971	-
m_T^e	170.461	204.792	149.850
p_T^μ	139.160	158.538	-
m_T^μ	195.963	191.303	170.817
$C_{lq}^{(3)}$ extrapolated	15.43	16.99	15.24

Table 6: Table of fitted slopes for different observable and the corresponding $C_{lq}^{(3)}$

4.3 Extrapolation of the Wilson coefficient

In the two last sections, we have shown the possibility to deceive a mass fit when the news physics coefficient is turned on. Now we will use the linear relations obtained to extrapolate the value of the Wilson coefficient that would be required to give the mass deviation obtained at the CDF II collaboration.

In the Tab. 6, we show the different slopes fitted for the five observables of interest. This is done for our 3 situations, parton level at 10 000 and 100 000 events as well as hadron level for 10 000 events. The deviation to the standard model prediction obtained at the Tevatron is 0.095 %. So we will determine the value of the coefficient needed by multiplying the deviation with the average of slopes for the three situations. We limit the analysis on deviation given by coefficient with χ^2 not too big. Hence, we choose $C_{lq}^{(3)} < |60|$ at both parton level and hadron level. The extrapolated Wilson coefficients are given in Tab. 6. We can see that the three results are close to each other and $C_{lq}^{(3)} \sim 15$. We note that we need $C_{lq}^{(3)} \sim 10$ to have a deviation of 0.001. Yet, by dimensional analysis, the modification should be around $m_W^2/\Lambda^2 \sim 0.01$. Therefore, there is roughly a factor of 100 between the two computations. We check that this is not related to the bounds of fit. Indeed, one can see on Fig.15 that for NP the shape is more spread than SM. However extending the fitting bounds does not increase significantly the sensitivity of the fit. One may argue that it could be related to the shape of the distribution. The variation of the SM vs SM case is more perky that the case SM vs NP and may be a part of the explanation. This should be another evidence that we are not working with the same hypothesis.

4.4 Constraints on the Wilson coefficient

In this section we compile different constraints at low and high energy on the Wilson coefficient. We check whether the extrapolated value matches with the different fit performed in the literature. We also discuss the possible effect of $C_{lq}^{(3)}$ on some Electroweak Precision Observable that would be modified by this Wilson coefficient. Indeed, if it modifies m_Z, m_H, α_{EM}, G_F or m_t it will modify the standard model prediction of the W-mass.

A From the [9], we can look at the computed deviations given in the literature,

$$\delta M_Z^2 \equiv \frac{1}{2\sqrt{2}} \frac{\hat{m}_Z^2}{\hat{G}_F} C_{HD} + \frac{2^{1/4}\sqrt{\pi}\sqrt{\hat{\alpha}}\hat{m}_Z}{G_F^{3/2}} C_{HWB}, \tag{34}$$

$$\delta G_F \equiv \frac{1}{\sqrt{2}\hat{G}_F}\left(\sqrt{2}C_{Hl}^{(3)} + \frac{C'_{ll}}{\sqrt{2}}\right), \tag{35}$$

$$\delta s^2(\hat{\theta}) \equiv -\frac{s_{\hat{\theta}}c_{\hat{\theta}}}{2\sqrt{2}\hat{G}_F(1-2s_{\hat{\theta}}^2)}\left[s_{\hat{\theta}}c_{\hat{\theta}}(C_{HD} + 4C_{Hl}^{(3)} - 2C'_{ll}) + 2C_{HWB}\right], \tag{36}$$

where $\hat{m}_Z^2$, $\hat{G}_F$ and $\hat{\alpha}_{EM}$ are input parameters. Note that $s_{\hat{\theta}} = sin(\hat{\theta})$ depends on $\hat{\alpha}_{EM}$ by

$$s_{\hat{\theta}}^2 = \frac{1}{2} - \frac{1}{2}\sqrt{1 - \frac{4\pi\hat{\alpha}_{EM}}{\sqrt{2}\hat{G}_F\hat{m}_Z^2}}. \tag{37}$$

As we can see, the $C_{lq}^{(3)}$ is not involved in Eq.34-36 and therefore not modified the parameters used to determine the W-mass in the standard model. We should also check that the mass of the Higgs and the mass of the top are not changed since it is involved in the radiative corrections (see Eq.22).

$$\delta M_H^2 = \hat{m}_H^2\left(-\frac{3C_H}{2\lambda} + 2C_{H\Box} - \frac{C_{HD}}{2}\right) \tag{38}$$

and the modification of the top Yukawa coupling is given as followed,

$$\delta g_{h\bar{f}f} = \frac{\hat{Y}_f}{\sqrt{2}}\left[\bar{v}_T^2\left(C_{H\Box} - \frac{C_{HD}}{4}\right) - \frac{\delta G_F}{\sqrt{2}}\right] - \frac{\bar{v}_T^2}{\sqrt{2}}C_{fH}^*, \tag{39}$$

where $\hat{Y}_f = 2^{3/4}\hat{m}_f\sqrt{\hat{G}_f}$ and $\delta v_T^2 = \bar{v}_T^2 - \hat{v}_T^2 = \frac{\delta G_F}{G_F}$. Here again the $C_{lq}^{(3)}$ is not involved in the shift of the parameters of interest in the precise determination of the W-mass in the standard model.

Even if the Wilson coefficient does not modify the parameters discussed above, we should verify whether this coefficient could affect the distributions used to determine their values. We begin with the Higgs mass, $m_H = 125.09 \pm 0.21 \pm 0.11\ GeV$, the channels considered when measuring its mass are $pp \to H \to \gamma\gamma$ and $pp \to H \to ZZ \to llll$ [4]. Here the possible modification is logarithmic and plays a role in the radiative corrections, so it should be negligible [5]. We now focus on the determination of $sin^2(\hat{\theta})$. Its value has been determined with precision by measuring the forward-backward asymmetry of the polar-angle distribution at the Tevatron by the CDF and D0 collaboration [14]. The procedure is similar to the one used to measure the mass of the W. These collaborations have generated a template of distributions by varying the value of $sin^2(\hat{\theta})$ and they have fitted with the experimental distributions. The expression of the forward-backward asymmetry is given by

$$A_{FB}(M) = \frac{\sigma_f(M) - \sigma_b(M)}{\sigma_f(M) + \sigma_b(M)}, \tag{40}$$

where σ_f (σ_b) is forward (backward) Drell-Yan cross-section for the lepton pair and M the invariant mass for $p\bar{p} \to \gamma^* \to l^-l^+$ and $p\bar{p} \to Z \to l^-l^+$. In this case, the Wilson coefficient has an impact on the determination of the $sin^2(\hat{\theta})$ and so the fine structure constant. However, there are other methods to determine its value without taking into account this contribution. An example is the absorption of photon by a rubidium atom. The measurement of the velocity recoil of the atoms can be used to determined with high precision the value of α [29]. The next parameter is the Fermi's constant, $G_F = 1.16637 \cdot 10^{-5}\ GeV^{-2}$, based on the muons decay,

$$\Gamma_\mu = \frac{(G_F^\mu)^2 m_\mu^5}{192\pi^3}(1 + \Delta q), \tag{41}$$

where m_μ is the muon's mass and Δq are phase space, QED and hadronic radiative corrections [20]. Since it is an interaction between lepton only, it is not affected by the Wilson coefficient. The 4th parameter is the Z mass, it has been precisely determined by process such as $e^+e^- \to Z \to f\bar{f}$ where $f\bar{f}$ are e^+e^-, $\mu^+\mu^-$, $\tau^+\tau^-$ and $q\bar{q}$ [16]. The coefficient is not involved in fully leptonic channels. Nevertheless, it should contribute to the last one, the production of $q\bar{q}$.
We now discuss the possible contributions of the Wilson coefficient to the mass of the top quark. It has been measured for three processes, $pp \to t\bar{t} \to hadronic$ [15], $pp \to t\bar{t} \to lv_l + jets$ [18] and $pp \to t\bar{t} \to WWb\bar{b} \to l^+l^-\nu_l\bar{\nu}_l b\bar{b}$ [13] [17]. The distributions for the first process are not modified because it is only hadronic. For the second process, both tops decay into bottoms and W-bosons. One W decays into lepton and neutrino and the other decays into $q\bar{q}$. Finally, we look at the di-lepton channel. In this channel two tops are created and decay to a W boson and a b quark. The W's will finally decay into charged leptons and their corresponding neutrinos. The $C_{lq}^{(3)}$ interfere with the standard model contribution as shown on Fig.19a-19b where an example of diagrams is shown. The top mass is determined by reconstructing the invariant mass of the lepton and the b-tagged jet. However, one can consider some symmetries that decouple the 3rd generation to the others. Nevertheless, it is possible to draw Feynman diagrams that produce the final state used to determine the mass of the top, as shown on Fig.19c. On this figure, we have shown the possible top pair-like event in the *dilepton* or $lepton + jet$ channel but with no tops produced.

We now move on the comparison with data. The first constraints, are obtained in [7], by looking at the following 4-fermion operators in order to parameterize di-lepton observables at LHC, di-electron and di-muon. The analysis is limited to the first generation of quarks and by imposing that the couplings in the lepton sector are universal among flavours and diagonal among generations. Madgraph is used to generate events and Pythia 6 and Delphes are in charge of hardronization and detector simulation respectively. The observable of interest is the lepton invariant mass and the analysis is performed up to Λ^4. They used the ATLAS and CMS di-lepton search at $\sqrt{s} = 8\,TeV$ for four bins[1] between $0.9 - 3\,TeV$. The bounds are obtained by turning on one operator at a time and by comparing the expected number of events in each bin to the data. The 95 % C.L. at $\frac{c_{lq}^{(3)}}{\Lambda^2}$ $[TeV^{-2}]$ is given by [-0.106, 0.019], where $\Lambda^2 \sim 3\,TeV$.

The second constraints come from the electroweak constraints, it consists of the same analysis as above but with electroweak precision data. This includes data coming from LEP2. The bounds at 95 % for $\frac{c_{lq}^{(3)}}{\Lambda^2}$ $[TeV^{-2}]$ are given by [-0.006, 0.012]. Therefore the combined bounds for both LHC and electroweak are [-0.006, 0.011] for 95 %.

Let's now consider another analysis given in [8] to set bounds on the Wilson coefficient. In this analysis, the authors have included NNLO (Next to Next Leading Order) QCD and NLO EW as well as Λ^2 and Λ^4 corrections. The Λ^4 is composed of squared of dimension-six operators and dimension-eight operators. The observable of interest is again the invariant mass and the new physics scale is set at $4\,TeV$. The fit is performed for bins[2] between $116\,GeV$ and $1.5\,TeV$ with the LHC pp collision data at $\sqrt{s} = 8\,TeV$. As shown on Fig.20 , the bounds are obtained at Λ^2 in blue and Λ^4 in red. The bounds at Λ^2 are $-(0.028 \pm 0.028)\,TeV^{-2}$ at 95 %.

[1] Bins : $0.9 - 1.3\,TeV$, $1.3 - 1.8\,TeV$, $1.8 - 3\,TeV$ for CMS and $1.2 - 3\,TeV$ for Atlas

[2] Bins : $116-130\,GeV$, $130-150\,GeV$, $150-175\,GeV$, $175-200\,GeV$, $200-230\,GeV$, $230-260\,GeV$, $260-300\,GeV$, $300 - 380\,GeV$, $380 - 500\,GeV$, $500 - 700\,GeV$, $700 - 1000\,GeV$, $1000 - 1500\,GeV$

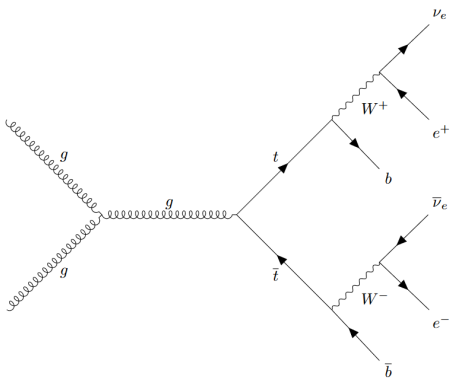

(a) Top pair production in SM

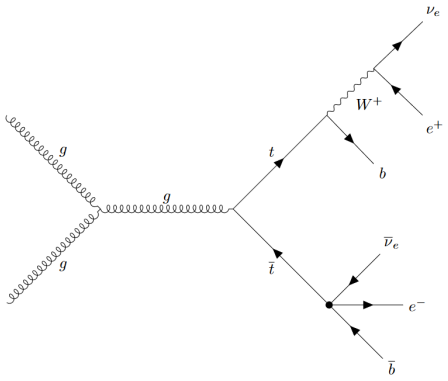

(b) Top pair production with $C_{lq}^{(3)}$

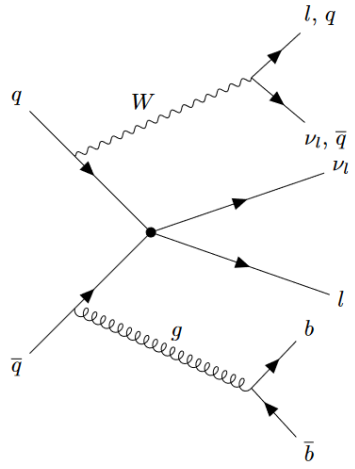

(c) Wrongly interpreted top pair production

Figure 19: Example of top pair-like events at the LHC with and without effective operator

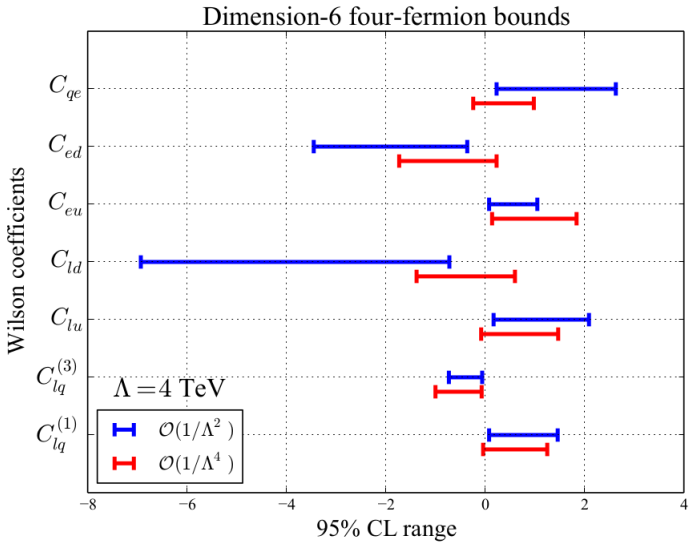

Figure 20: 95 % CL intervals up to Λ^{-2} and Λ^{-4} for four-fermion operators

In the previous paragraph, we have discussed the limit on the Wilson coefficient at high energy. We move now on constraints coming from bounds at low energy. If we look at the β decay we can determine the value of the Fermi's constant and compare it to the one determined by the muons decay. In the universal limit, where the dimension-six operator are invariant under $U(3)_q \times U(3)_u \times U(3)_d \times U(3)_l \times U(3)_e$, the deviation to the CKM unitarity is given by,

$$\delta|V_{CKM}|^2 = \frac{\sqrt{2}}{\hat{G}_F}\left(-C_{lq}^{(3)} + C'_{ll} + C_{Hq}^{(3)} - C_{Hl}^{(3)}\right) \tag{42}$$

Compared to the deviation resumed in Eq.35-39, the deviation depends now on the value of the $C_{lq}^{(3)}$. In [11], the authors include the beta decay data to the EWPO fit and derived bounds on this coefficient. The bounds on $C_{lq}^{(3)}$ are now given by $-(0.082 \pm 0.045)\ TeV^{-2}$.

Moreover, one may finaly look at the "oblique" parameters. These parameters, firstly introduced by M. Peskin and T. Takeuchi in 1992 [31], parameterised the effect of new physics in the vacuum polarization energy of the gauge bosons. Up to order p^2, for the SMEFT there are three parameters (S, T, U) that are not related to the Wilson coefficient. At p^4 order, there are 4 other parameters (X, Y, V, W), where one could be related to $C_{lq}^{(3)}$ in the $U(3)^5$ symmetric case,

$$C_{lq}^{(3)} = -\alpha W. \tag{43}$$

where α is the fine structure constant [23]. In [22], one can find a constraint at low energy on W and therefore the Wilson coefficient. The scale of new physics is given by $\Lambda = v$ and $W = (-0.01 \pm 0.08)\ TeV^{-2}$.

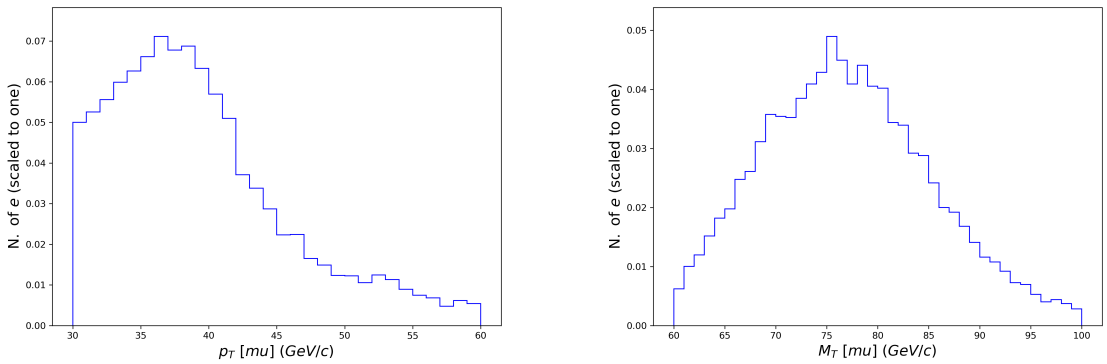

(a) p_T^{μ} (b) m_T^{μ}

Figure 21: Distributions at hadron level after the detector simulation

As we have seen above, the constraints on the Wilson coefficient are, at least, two orders lower than the value requested to give the right deviation observed at CDF II collaboration. This implies that even if we have shown that the presence of an effective operator can deceive a mass fit, its coefficient is far too big to be responsible of it. Indeed, if we take the biggest upper bound and inverses the analysis to find the mass shift, it should be in the order of the keV. In other words, it is supposed to sit three orders below that the standard deviation of the measured and predicted W-mass. Finally, Atlas collaboration at CERN published a note on a similar analysis of there data obtained at the LHC with pp collisions at $\sqrt{s} = 7\ TeV^{-2}$. They measured a mass of $m_W = 80.360 \pm 0.016\ GeV$ which is consistent with the standard model prediction [27].

Finally, we discuss the transverse mass distributions at hadron level that we have used. The shape of distributions does not really look like the ones given in the ATLAS and CDF II papers (Ref.[1], [26] and [27]). The definition of the missing transverse energy of Madanalysis is just the different neutrinos. Whereas in those references the definition is different,

$$\vec{p}_T{}^{\nu} = -\vec{p}_T{}^{l} + \vec{u} \tag{44}$$

where $\vec{u}$ is the hadronic recoil and $\vec{p}_T{}^{\nu}$ the missing transverse energy. The definition of the transverse mass is also different from the Madanalysis one,

$$m_T = \sqrt{2(p_T^{2\,l} p_T^{2\,\nu} - \vec{p}_T{}^{l}\vec{p}_T{}^{\nu})}. \tag{45}$$

We have performed a detector simulation with DELPHES 3 [24] and plotted the computed distributions on Fig.21. As we can see on Fig21a, the distributions of transverse momentum are not modified compared to the one given on Fig.9f. However, the distribution for transverse mass is modified (see Fig.21b).

5 Conclusion

In April 2022, the CDF II collaboration has published, a new measurement of the W mass performed at Tevatron. This measurement turned out to be in tension with the standard model prediction. This has raised a lot of concern from the scientific community since the W boson mass is an important parameter in the standard model. Indeed, the W mass prediction is highly sensitive to new physics. Despite discussions on the validity of the result itself, we have studied the effect of new physics on the determination of this mass.

Firstly, we have talked about the standard model of particle physics that explained three of the four fundamental interactions at the microscopic level. Despite its successful story, it is well known that it is not complete. In colliders physics, one commonly assume that new physics takes place at higher energy. The effect at low energy of new physics can be inferred by Effective Field Theories. Hence, we have developed the concepts of EFT's, the Fermi's theory as an historical example and the Standard Model Effective Field Theory.
We have continued with an historical recap of the W boson and its mass measurement and prediction. The following section was devoted to a presentation of the Tevatron and the CDF II collaboration as well as the presentation of the new mass measurement. Then, we have talked about the theoretical effect of a semileptonic four-fermion operator on standard model distributions used to determine the mass of the W boson.

Secondly, we have built the model by expanding the standard model with only one semileptonic four-fermion operator. We have implemented the model into madgraph and generated standard model and new physics distributions. The observables chosen where transverse momentum for electrons, muons and missing energy as well as transverse mass for muons and electrons. In order to fit distributions together, we applied restrictive cuts on the transverse momentum. This fit takes the same idea as the one used by the CDF II collaboration, the "template" method. This fit allowed us to determine the best fitted mass and its corresponding confidence interval at parton level for all observables and at hadron level for transverse masses.

Thirdly, we have presented the results at both parton and hadron level. In the first case, we have seen an increase of the fitted mass as the Wilson coefficient was increasing. We have noted that the theoretical mass of the W boson was excluded by five sigmas when $C_{lq}^{(3)}$ was bigger than 40. We have observed an increase of the χ^2_{min} which denoted that the fit was less efficient. This was expected since we are further and further from the standard model hypothesis. We have also illustrated the clear modification of shape of the new physics distribution compare to the standard model ones with modified m_W. After neglecting Λ^4 contribution, we have verified the linearity of the model. To conclude with the parton level, we have performed the analysis with 10 times the number of events simulated. We have got the same results as above and have reduced the numerical noise by approximately three. In the second case, the hadron level, we have performed the same analysis as at parton level but for only transverse masses. We have observed this increasing of the fitted mass as $C_{lq}^{(3)}$ but have excluded the theoretical mass for $C_{lq}^{(3)} = 60$. The increasing of the χ^2_{min} has been noted and the linearity verified.

Finally, we have investigated the possible effect on the measurement of parameters used to predict the mass of the W boson. No deviation of these parameters depends on $C_{lq}^{(3)}$. Nevertheless, the only

measurement not affected by the operator is the Fermi's constant. The others have been discussed separately. We have computed the value of the Wilson coefficient needed to get the deviation observed by the CDF II collaboration. We have checked the validity of this Wilson coefficient by looking at the constants given in the literature. All constraints considered are at least two orders of magnitude smaller than the coefficient needed. This means that the required Wilson coefficient are excluded by data. Consequently, in this analysis, we have not been able to prove that the mass anomaly could be related to new physics contribution.

References

[1] T. Aaltonen et al. "A precise measurement of the W-boson mass with the Collider Detector at Fermilab". In: *Physical Review D* 89.7 (Apr. 3, 2014), p. 072003. ISSN: 1550-7998, 1550-2368. DOI: 10.1103/PhysRevD.89.072003. arXiv: 1311.0894[hep-ex]. URL: http://arxiv.org/abs/1311.0894.

[2] Adam Alloul et al. "FeynRules 2.0 - A complete toolbox for tree-level phenomenology". In: *Computer Physics Communications* 185.8 (Aug. 2014), pp. 2250–2300. ISSN: 00104655. DOI: 10.1016/j.cpc.2014.04.012. arXiv: 1310.1921[hep-ph]. URL: http://arxiv.org/abs/1310.1921.

[3] J. Alwall et al. "The automated computation of tree-level and next-to-leading order differential cross sections, and their matching to parton shower simulations". In: *Journal of High Energy Physics* 2014.7 (July 2014), p. 79. ISSN: 1029-8479. DOI: 10.1007/JHEP07(2014)079. arXiv: 1405.0301[hep-ph]. URL: http://arxiv.org/abs/1405.0301.

[4] ATLAS and C. M. S. Collaborations. "Combined Measurement of the Higgs Boson Mass in pp Collisions at $\sqrt{s}=7$ and 8 TeV with the ATLAS and CMS Experiments". In: *Physical Review Letters* 114.19 (May 14, 2015), p. 191803. ISSN: 0031-9007, 1079-7114. DOI: 10.1103/PhysRevLett.114.191803. arXiv: 1503.07589[hep-ex]. URL: http://arxiv.org/abs/1503.07589.

[5] M. Awramik et al. "Precise Prediction for the W-Boson Mass in the Standard Model". In: *Physical Review D* 69.5 (Mar. 17, 2004), p. 053006. ISSN: 1550-7998, 1550-2368. DOI: 10.1103/PhysRevD.69.053006. arXiv: hep-ph/0311148. URL: http://arxiv.org/abs/hep-ph/0311148.

[6] Cesare Bini. "Data analysis in Particle Physics". In: (2016). URL: https://www.roma1.infn.it/~bini/StatEPP_new.pdf.

[7] J. de Blas, M. Chala, and Jose Santiago. "Global Constraints on Lepton-Quark Contact Interactions". In: *Physical Review D* 88.9 (Nov. 13, 2013), p. 095011. ISSN: 1550-7998, 1550-2368. DOI: 10.1103/PhysRevD.88.095011. arXiv: 1307.5068[hep-ex,physics:hep-ph]. URL: http://arxiv.org/abs/1307.5068.

[8] Radja Boughezal, Emanuele Mereghetti, and Frank Petriello. "Dilepton production in the SMEFT at $\mathcal O(1/\Lambda^4)$". In: *Physical Review D* 104.9 (Nov. 29, 2021), p. 095022. ISSN: 2470-0010, 2470-0029. DOI: 10.1103/PhysRevD.104.095022. arXiv: 2106.05337[hep-ph]. URL: http://arxiv.org/abs/2106.05337.

[9] Ilaria Brivio and Michael Trott. "The Standard Model as an Effective Field Theory". In: *Physics Reports* 793 (Feb. 2019), pp. 1–98. ISSN: 03701573. DOI: 10.1016/j.physrep.2018.11.002. arXiv: 1706.08945[hep-ph]. URL: http://arxiv.org/abs/1706.08945.

[10] Neil D. Christensen and Claude Duhr. "FeynRules - Feynman rules made easy". In: *Computer Physics Communications* 180.9 (Sept. 2009), pp. 1614–1641. ISSN: 00104655. DOI: 10.1016/j.cpc.2009.02.018. arXiv: 0806.4194[hep-ph]. URL: http://arxiv.org/abs/0806.4194.

[11] Vincenzo Cirigliano et al. "Beta-decay implications for the W-boson mass anomaly". In: *Physical Review D* 106.7 (Oct. 3, 2022), p. 075001. ISSN: 2470-0010, 2470-0029. DOI: 10.1103/PhysRevD.106.075001. arXiv: 2204.08440[hep-ph,physics:nucl-th]. URL: http://arxiv.org/abs/2204.08440.

[12] ATLAS Collaboration. "Measurement of the W-boson mass in pp collisions at $\sqrt{s}=7$ TeV with the ATLAS detector". In: *The European Physical Journal C* 78.2 (Feb. 2018), p. 110. ISSN: 1434-6044, 1434-6052. DOI: 10.1140/epjc/s10052-017-5475-4. arXiv: 1701.07240[hep-ex]. URL: http://arxiv.org/abs/1701.07240.

[13] ATLAS Collaboration. "Measurement of the top quark mass in the $t\bar{t}\to$ dilepton channel from $\sqrt{s}=8$ TeV ATLAS data". In: *Physics Letters B* 761 (Oct. 2016), pp. 350–371. ISSN: 03702693. DOI: 10.1016/j.physletb.2016.08.042. arXiv: 1606.02179[hep-ex]. URL: http://arxiv.org/abs/1606.02179.

[14] CDF Collaboration and D0 Collaboration. "Tevatron Run II combination of the effective leptonic electroweak mixing angle". In: *Physical Review D* 97.11 (June 28, 2018), p. 112007. ISSN: 2470-0010, 2470-0029. DOI: 10.1103/PhysRevD.97.112007. arXiv: 1801.06283[hep-ex]. URL: http://arxiv.org/abs/1801.06283.

[15] CMS Collaboration. "Measurement of the top-quark mass in all-jets t t-bar events in pp collisions at sqrt(s) = 7 TeV". In: *The European Physical Journal C* 74.4 (Apr. 2014), p. 2758. ISSN: 1434-6044, 1434-6052. DOI: 10.1140/epjc/s10052-014-2758-x. arXiv: 1307.4617[hep-ex]. URL: http://arxiv.org/abs/1307.4617.

[16] The ALEPH Collaboration et al. "Precision Electroweak Measurements on the Z Resonance". In: *Physics Reports* 427.5 (May 2006), pp. 257–454. ISSN: 03701573. DOI: 10.1016/j.physrep.2005.12.006. arXiv: hep-ex/0509008. URL: http://arxiv.org/abs/hep-ex/0509008.

[17] The CMS Collaboration. "Measurement of the top-quark mass in t t-bar events with dilepton final states in pp collisions at sqrt(s)=7 TeV". In: *The European Physical Journal C* 72.10 (Oct. 2012), p. 2202. ISSN: 1434-6044, 1434-6052. DOI: 10.1140/epjc/s10052-012-2202-z. arXiv: 1209.2393[hep-ex]. URL: http://arxiv.org/abs/1209.2393.

[18] The CMS Collaboration. "Measurement of the top-quark mass in t t-bar events with lepton+jets final states in pp collisions at sqrt(s) = 7 TeV". In: *Journal of High Energy Physics* 2012.12 (Dec. 2012), p. 105. ISSN: 1029-8479. DOI: 10.1007/JHEP12(2012)105. arXiv: 1209.2319[hep-ex]. URL: http://arxiv.org/abs/1209.2319.

[19] Eric Conte, Benjamin Fuks, and Guillaume Serret. "MadAnalysis 5, a user-friendly framework for collider phenomenology". In: *Computer Physics Communications* 184.1 (Jan. 2013), pp. 222–256. ISSN: 00104655. DOI: 10.1016/j.cpc.2012.09.009. arXiv: 1206.1599[hep-ph]. URL: http://arxiv.org/abs/1206.1599.

[20] Andreas Crivellin, Martin Hoferichter, and Claudio Andrea Manzari. "Fermi Constant from Muon Decay Versus Electroweak Fits and Cabibbo-Kobayashi-Maskawa Unitarity". In: *Physical Review Letters* 127.7 (Aug. 10, 2021). Publisher: American Physical Society, p. 071801. DOI: 10.1103/PhysRevLett.127.071801. URL: https://link.aps.org/doi/10.1103/PhysRevLett.127.071801.

[21] Luca Di Luzio, Ramona Gröber, and Paride Paradisi. "Higgs physics confronts the M_W anomaly". In: *Physics Letters B* 832 (Sept. 2022), p. 137250. ISSN: 03702693. DOI: 10.1016/j.physletb.2022.137250. arXiv: 2204.05284[hep-ex,physics:hep-ph]. URL: http://arxiv.org/abs/2204.05284.

[22] Adam Falkowski, Martín González-Alonso, and Kin Mimouni. "Compilation of low-energy constraints on 4-fermion operators in the SMEFT". In: *Journal of High Energy Physics* 2017.8 (Aug. 2017), p. 123. ISSN: 1029-8479. DOI: 10.1007/JHEP08(2017)123. arXiv: 1706.03783[hep-ex,physics:hep-ph]. URL: http://arxiv.org/abs/1706.03783.

[23] Adam Falkowski and Kin Mimouni. "Model independent constraints on four-lepton operators". In: *Journal of High Energy Physics* 2016.2 (Feb. 2016), p. 86. ISSN: 1029-8479. DOI: 10.1007/JHEP02(2016)086. arXiv: 1511.07434[hep-ph]. URL: http://arxiv.org/abs/1511.07434.

[24] J. de Favereau et al. "DELPHES 3, A modular framework for fast simulation of a generic collider experiment". In: *Journal of High Energy Physics* 2014.2 (Feb. 2014), p. 57. ISSN: 1029-8479. DOI: 10.1007/JHEP02(2014)057. arXiv: 1307.6346[hep-ex,physics:hep-ph]. URL: http://arxiv.org/abs/1307.6346.

[25] *Fermilab | Tevatron | Accelerator*. URL: https://www.fnal.gov/pub/tevatron/tevatron-accelerator.html (visited on 05/07/2023).

[26] *High-precision measurement of the W boson mass with the CDF II detector*. DOI: 10.1126/science.abk1781. URL: https://www.science.org/doi/10.1126/science.abk1781.

[27] *Improved W boson Mass Measurement using 7 TeV Proton-Proton Collisions with the ATLAS Detector*. Place: Geneva. 2023. URL: http://cds.cern.ch/record/2853290.

[28] Aneesh V. Manohar. *Introduction to Effective Field Theories*. Apr. 16, 2018. DOI: 10.48550/arXiv.1804.05863. arXiv: 1804.05863[hep-ph]. URL: http://arxiv.org/abs/1804.05863.

[29] Léo Morel et al. "Determination of the fine-structure constant with an accuracy of 81 parts per trillion". In: *Nature* 588.7836 (Dec. 2020). Number: 7836 Publisher: Nature Publishing Group, pp. 61–65. ISSN: 1476-4687. DOI: 10.1038/s41586-020-2964-7. URL: https://www.nature.com/articles/s41586-020-2964-7.

[30] Particle Data Group et al. "Review of Particle Physics". In: *Progress of Theoretical and Experimental Physics* 2020.8 (Aug. 14, 2020), p. 083C01. ISSN: 2050-3911. DOI: 10.1093/ptep/ptaa104. URL: https://academic.oup.com/ptep/article/doi/10.1093/ptep/ptaa104/5891211.

[31] Michael E. Peskin and Tatsu Takeuchi. "Estimation of oblique electroweak corrections". In: *Physical Review D* 46.1 (July 1, 1992). Publisher: American Physical Society, pp. 381–409. DOI: 10.1103/PhysRevD.46.381. URL: https://link.aps.org/doi/10.1103/PhysRevD.46.381.

[32] Chris Quigg. *Gauge Theories of the Strong, Weak, and Electromagnetic Interactions: Second Edition*. STU - Student edition. Princeton University Press, 2013. ISBN: 978-0-691-13548-9. URL: https://www.jstor.org/stable/j.ctt3fgx94.

[33] Juan Rojo. "The Standard Model Effective Theory: towards a pedagogical primer". In: (Feb. 4, 2020). URL: https://juanrojocom.files.wordpress.com/2020/02/smeft-drstp-2.pdf.

[34] Torbjörn Sjöstrand et al. "An Introduction to PYTHIA 8.2". In: *Computer Physics Communications* 191 (June 2015), pp. 159–177. ISSN: 00104655. DOI: 10.1016/j.cpc.2015.01.024. arXiv: 1410.3012[hep-ph]. URL: http://arxiv.org/abs/1410.3012.

[35] *Standard Model of Elementary Particles*. URL: https://upload.wikimedia.org/wikipedia/commons/0/00/Standard_Model_of_Elementary_Particles.svg (visited on 05/07/2023).

[36] Mark Thomson. *Modern Particle Physics*. Higher Education from Cambridge University Press. ISBN: 9781139525367 Publisher: Cambridge University Press. Sept. 5, 2013. DOI: 10.1017/CBO9781139525367. URL: https://www.cambridge.org/highereducation/books/modern-particle-physics/CDFEBC9AE513DA60AA12DE015181A948.

[37] Inc. Wolfram Research. *Mathematica*. Version Version 13.2. Champaign, Illinois, 2022. URL: https://www.wolfram.com/mathematica.

UNIVERSITE CATHOLIQUE DE LOUVAIN

Faculté des sciences

Place des sciences, 2 bte L6.06.01, 1348 Louvain-la-Neuve, Belgique | **www.uclouvain.be/sc**